

## Photonic band structure of cholesteric elastomers

P. A. Bermel and M. Warner

*Cavendish Laboratory, University of Cambridge, Madingley Road, Cambridge CB3 0HE, United Kingdom*

(Received 16 October 2001; revised manuscript received 19 February 2002; published 16 May 2002)

We calculate the photonic band structure along and oblique to the helix axis of cholesteric elastomers. They are highly deformable, self-assembling systems. They display brilliantly colored reflections and lasing owing to stop bands in their photonic band structure. This band structure varies sensitively and extensively with strain. We show how additional stop bands open up and how they all shift in frequency. We predict a “total” stop band, that is, for both circular polarizations and show analytically how stop bands scale with strain. The extension of stop bands to a range of angles thereby creates pseudogaps, and the relevance to low-threshold lasing is discussed.

DOI: 10.1103/PhysRevE.65.056614

PACS number(s): 42.70.Qs, 61.30.-v, 81.40.Jj

### I. INTRODUCTION

Photonic band materials (PBMs) interact with light analogously to the way semiconductors interact with electrons—via the periodic modulation of dielectric properties on a length scale matching the wavelengths of the quanta of interest. Light is manipulated by the structure rather than by underlying atomic or molecular properties. Structures can be manufactured; for instance, Yablonovitch and Gmitter constructed an fcc photonic crystal by drilling holes into a dielectric medium [1]. Later, Ozbay and co-workers designed a picket fence structure, which is assembled by stacking two-dimensional (2D) layers [2].

Self-assembling PBMs are preferred at optical and near-infrared wavelengths. Several examples include air holes in a titania matrix [3], copolymer-homopolymer films that form lamellar structures [4], thin films of polymethylmethacrylate infilled with  $\text{SnS}_2$  [5]. Cholesteric liquid crystals (CLCs) [6–10] are classical PBMs. Their brilliant colors are well known and arise from a periodic *twisting* of their anisotropic dielectric properties, distinct from the systems mentioned above. Local orientational ordering along a director  $\mathbf{n}$  rotates as a periodic function of distance along the pitch axis  $z$ . The director of an ideal CLC advances uniformly, tracing out a helix of pitch  $p_0$ , which can be adjusted to match the wavelength of visible light. At normal incidence, circularly polarized light that twists in the same sense as a helix is reflected with its original polarization, while circularly polarized light that twists in the opposite sense is transmitted unchanged. By solving Maxwell’s equations in a rotating frame, de Vries found a single stop band, a one-dimensional band gap in the photonic structure [6]. We shall additionally be concerned with oblique incidence, and also in the effects of external fields on modifying cholesteric spirals and hence their band structures.

PBMs have unique properties, which have spurred interest in their design. In an early exposition of electromagnetic band structure, John also suggested how light can be localized [11]. The spontaneous emission spectrum from atoms and molecules can be modified in these materials [12–14], leading among other things to low-threshold lasing: Yablonovitch [13] predicted that the lasing threshold would be decreased by introducing a defect into an otherwise perfect

photonic material. Spontaneous emission is suppressed in the bulk and excitation would not be drained by any emission into nonlasing modes. Such low-threshold lasing has recently been observed in two-dimensional photonic crystals [15]. Alternatively, one can design lasers that take advantage of the enhanced dwell time associated with the band edge divergence of the density of states [16]. Indeed, experimentally, the first observations of this type of lasing was in CLCs, by Kopp *et al.* [17] and by Taheri and Palfy-Muhoray [18]. Kopp *et al.* showed that the lasing was at the stop band edges and not, as expected, at the center where the reflection was largest. The band structures we predict, especially away from normal incidence, add weight to their analysis and findings. Lasing has subsequently also been seen in cholesteric elastomers (CEs) [19]. CEs are made by cross-linking cholesteric polymer liquid crystals [20] to form defect-free monodomain rubber strips tens of centimeters long. They display spectacular opticomechanical effects, viz., large changes in the frequencies of reflection and of lasing [19] in response to imposed mechanical strains.

Our calculations on CEs point to phenomena and applications that are not possible in existing photonics, and hitherto unsuspected in the liquid crystal field. For instance, we find multiple 1D band gaps, some not at the zone edges, in contrast to classical CLCs. We also observe gaps for light of the opposite handedness to the underlying helix, again unexpected in classical CLC systems. At some directions the gaps for both polarizations overlap in frequency, giving a total stop band of significance when polarization control is required. Our systems are highly deformable (many-fold) and we shall find shifts in the (developing) band structure that can be large [19–21].

By contrast, existent photonic media (noncholesteric) typically have piecewise variation of a typically isotropic refractive index in going between a matrix and its inclusions. In one theoretical proposal and calculation, Busch and John [22] considered nematic liquid crystals filling an inverse opal structure. The voids in the skeleton thereby had an anisotropic refractive index, as in our case, and we closely follow the analysis that was introduced there to deal with the added complexity of the tensorial structure to the dielectric constant and thus also with polarization effects. Busch and John proposed applying fields to the nematic liquid to redirect the director and thereby tune the contrast with the various crys-

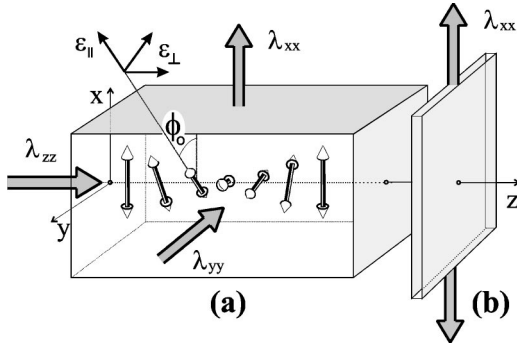


FIG. 1. Schematic diagrams of (a) an expanded view of a section of a strip of elastomer showing its cholesteric director distribution. The director twists periodically along the pitch axis, here the  $z$  axis in each case. For the elastic strip,  $z$  is perpendicular to the flat face. Cholesterics are approximately optically uniaxial, with dielectric constants  $\epsilon_{\parallel}$  shown along the nematic order, and  $\epsilon_{\perp}$  in the perpendicular plane. Elements of the deformation gradient tensor (for the solid case)  $\underline{\lambda}$  are shown:  $\lambda_{xx}$ , a stretch applied in the  $x$  direction,  $\lambda_{zz}$  and  $\lambda_{yy}$  are the attendant contractions along  $z$  and  $y$ , respectively. (b) The geometry of the strip, (a) being a section from this.

tallographic directions and thus to create gaps. However piecewise dielectric continuity is retained and the direction of anisotropy is homogeneous in the whole crystal. By contrast, CLC's have a continuous variation of the principal axes of birefringence—which corresponds to a continuously rotating coordinate frame. The principal axes guide the waves along a generally nontrivial, periodic path and give rise to sharply different behaviors for each polarization. Polarization effects are thus very subtle and become more so for oblique incidence. Control of polarization is at the heart of LC and optical devices; we thus view this work as a step toward fresh classes of photonic solids with deformable, tunable band structures highly sensitive to polarization.

We first describe how CEs deform and how their director distribution is coarsened from an initially ideal helix. This creation of additional harmonics in the dielectric distribution (the “photonic potential” in an analogy to semiconductors) is what creates the additional stop bands and, in part, their extensions to oblique incidence. We then sketch the classical (normal incidence) photonics of cholesterics before calculating the 3D band structure in both the ideal and distorting systems. We draw a contrast between the photonic structure of distorting elastomers and that of liquids with external magnetic fields applied.

## II. CHOLESTERIC STRUCTURES OF DEFORMING LIQUIDS AND SOLIDS

A cholesteric locally has nematic (orientational) ordering along a director  $\mathbf{n}$ , which rotates as a periodic function of distance along the pitch axis  $z$ , as illustrated in Fig. 1(a) (which will also serve to illustrate strains applied to CEs),

$$\mathbf{n} = \cos(q_0 z) \hat{x} + \sin(q_0 z) \hat{y}. \quad (1)$$

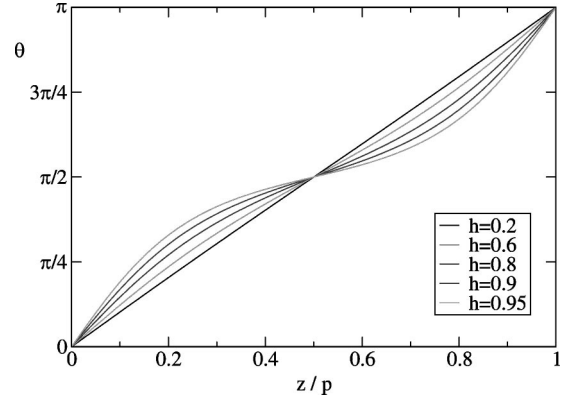


FIG. 2. Angular orientation of the director  $\theta$  versus the reduced position  $\tilde{z} = z/p$  for several values of the reduced field  $h = H/H_c$ .

The director of an ideal cholesteric advances uniformly, tracing out a helix of pitch  $p_0 = 2\pi/q_0$ . Such a distribution is created by molecules with a handedness inducing a twist, that is, the Frank twist elastic energy density  $\frac{1}{2}K_2[\mathbf{n} \cdot (\nabla \times \mathbf{n}) + q_0]^2$  will be minimized when  $\mathbf{n} \cdot (\nabla \times \mathbf{n}) = -q_0$ .  $K_2$  is the Frank twist elastic constant.

A cholesteric can be considered approximately locally uniaxial, with an anisotropic permittivity, for instance, dielectric,  $\epsilon_{\parallel}$  along  $\mathbf{n}$  and  $\epsilon_{\perp}$  perpendicular to  $\mathbf{n}$ .

*Cholesteric liquids.* The twisted structure of a cholesteric liquid can be unwound by a magnetic (or electric) field applied perpendicular to the helix axis, a classical problem first considered by Meyer [7] and by de Gennes [8], see also Dreher [23] for the case of finite samples with boundary conditions. Consider a magnetic field  $H$  along the  $y$  direction. Since cholesterics have an anisotropic magnetic susceptibility  $\chi_a = \chi_{\parallel} - \chi_{\perp}$ , the magnetic energy is  $F_{\text{ext}} = -\frac{1}{2} \int d\mathbf{r} \chi_a (\mathbf{H} \cdot \mathbf{n})^2$ . The helix untwists (increasing the period) and coarsens until the energy gain from aligning with the field balances the Frank penalty for deviations from the original structure. The director orientations coarsen, as in Fig. 2, but with the  $z$  coordinate being reduced to  $\tilde{z}$  by a *lengthening period* (but see [23]). At a critical field  $H_c = (\pi q_0/2) \sqrt{K_2/\chi_a}$ , the period diverges logarithmically as the entire sample aligns with the external field. For typical cholesteric liquids with a pitch of 20  $\mu\text{m}$ ,  $H_c = 15\,000$  G and  $E_c = 50$  s V/cm. The characteristic length  $\xi \equiv H^{-1} \sqrt{K_2/\chi_a}$ , a liquid cholesteric magnetic penetration depth, arises from the interplay between magnetic and Frank energies.  $\xi$  is comparable to the wavelength of visible light, thus giving rise to interesting photonic-magnetic-field effects in liquids. The central idea is the same as in our work on elastomers: distorted cholesteric structures have harmonics introduced into their director fields and thus higher-order effects in their band structure.

Chou *et al.* [9] first considered the effect of these distortions on the cholesteric photonic structure, see also Dreher [24] and Shtrikman and Tur [25]. We shall compare with their (normal) calculation when calculating the changing band structure of cholesteric elastomers under strain. One needs the variation of the director angle with  $z$  in order to calculate the photonics. Differences from CEs under strain are detailed in [26,27]. One important difference is that the

penetration depth arises from the competition between elastic and Frank energies. It is much shorter than  $\xi$  in liquids with the effect that we can ignore Frank elasticity for the solid systems.

*Cholesteric elastomers.* Nematic polymers are elongated (in the prolate case) by their surrounding nematic order. They are distributed as anisotropic random walks with mean square extents  $\langle R_i R_j \rangle = \frac{1}{3} \ell_{ij} \mathcal{L}$ , where there are effective step lengths parallel and perpendicular to the director and thus an effective step length tensor describing its Gaussian distribution

$$\ell_{ij} = (\ell_{\parallel} - \ell_{\perp}) n_i n_j + \ell_{\perp} \delta_{ij}, \quad (2)$$

and  $\mathcal{L}$  is the total contour length of the chain between cross links. Being Gaussians, the chains are capable of huge extensions and, therefore, the rubber they compose when cross linked will be too.

One can easily show, by analogy with classical rubber elasticity, that the free-energy density of a rubber composed of such chains is

$$F = \frac{1}{2} \mu \text{Tr}(\underline{\underline{\ell}}_0 \lambda^T \underline{\underline{\ell}}^{-1} \lambda), \quad (3)$$

where  $\mu$  is the shear modulus when the rubber is in the isotropic phase ( $\mu = n_x k_B T$ , where  $n_x$  is the number of such chains per unit volume).  $\underline{\underline{\ell}}_0$  represents the distribution locally at the time of formation of the elastomer,  $\underline{\underline{\ell}}$  represents it after distortion, for instance, if the director has rotated in response, so will  $\underline{\underline{\ell}}$ . Since the director rotates through the initial structure and (perhaps differently) through that after deformation, the energy density will be a function of position  $z$  along the pitch. The deformation tensor is  $\underline{\underline{\lambda}}$ , for instance,  $\lambda_{xx}$  is the stretch in the  $x$  direction (the new length divided by the old length in the  $x$  direction). Since rubber is a soft solid, deformations are at constant volume, that is  $\det(\underline{\underline{\lambda}}) = 1$ .

We shall consider imposed stretches of magnitude  $\lambda$  in the  $x$  direction, allowing constant volume contractions in the two perpendicular directions and suppressing shears (in this geometry they cost an energy that scales linearly with the sample size—in the thermodynamic limit, they are forbidden; see [26,27] for more details). Thus

$$\underline{\underline{\lambda}} = \begin{pmatrix} \lambda & 0 & 0 \\ 0 & \lambda_{yy} & 0 \\ 0 & 0 & \frac{1}{\lambda \lambda_{yy}} \end{pmatrix}. \quad (4)$$

By construction,  $\det(\underline{\underline{\lambda}}) = 1$ ; however, contractions in the  $y$  and  $z$  directions will be different, in general, since these two directions differ in their symmetry.

For a cholesteric rubber, one substitutes the CLC director distribution equation (1) into Eq. (2) for the initial effective step length tensor to obtain an explicit variation (which will resemble the later distribution of the dielectric constant, a related second-rank tensor that follows the rotating nematic order),

$$\underline{\underline{\ell}}_0 = \ell_{\perp} \left[ \underline{\underline{\delta}} + (r-1) \begin{pmatrix} \cos^2 \phi_0 & \cos \phi_0 \sin \phi_0 & 0 \\ \cos \phi_0 \sin \phi_0 & \sin^2 \phi_0 & 0 \\ 0 & 0 & 0 \end{pmatrix} \right]. \quad (5)$$

We have extracted a factor of  $\ell_{\perp}$  from  $\underline{\underline{\ell}}_0$ , which we shall hereafter neglect since it cancels with the inverse factor of  $\ell_{\perp}^{-1}$ , which we extract from  $\underline{\underline{\ell}}^{-1}$  that appears multiplicatively with  $\underline{\underline{\ell}}_0$  in the free-energy density (3). The ratio  $r = \ell_{\parallel} / \ell_{\perp}$  thereafter characterizes the  $\underline{\underline{\ell}}$  tensors and is a measure of the anisotropy of the chains. For instance, it determines the spontaneous distortion of elastomers when they enter the nematic state,  $\lambda_s = r^{1/3}$ . The anisotropy is in the range of  $r \sim 1.1$ –50 depending upon the types of chains making up the elastomer.

We show in an appendix how the transverse contractions take up highly nonclassical forms  $\lambda_{yy} \sim \lambda^{-5/7}$  and  $\lambda_{zz} \sim \lambda^{-2/7}$  on imposition of a stretch  $\lambda$  along  $x$ . In particular, convection of the cholesteric structure along with  $\lambda_{zz}$  gives an increase of the cholesteric wave vector  $q = q_0 / \lambda_{zz} = q_0 \lambda^{2/7}$ . This is the first aspect of a deformable band structure that emerges: the fundamental stop band, and any features in the band structure created by distortion, will also shift in wave vector with  $\lambda^{2/7}$ . Thus the change of color and lasing toward the violet on stretching that has been observed in CEs is easily explained.

We also sketch in the Appendix how to calculate the variation of the director angle with distance  $z$  along the helix axis as an  $x$  strain  $\lambda$  is imposed, see also [26,27] for details. The result for  $\phi(z)$  in terms of the original angle  $\phi_0 = q_0 z$  is

$$\tan 2\phi = \frac{2(r-1)\lambda \lambda_{yy} \sin 2\phi_0}{(r-1)(\lambda^2 + \lambda_{yy}^2) \cos 2\phi_0 + (r+1)(\lambda^2 - \lambda_{yy}^2)}. \quad (6)$$

The initially helical director structure coarsens to that dominated by regions of slowly varying angles, separated by increasingly sharp twist walls [26,27]; see Fig. 3.

It is this nonuniform rotation of the director that gives the higher harmonics that generate the additional features in the photonic band structure as strain is imposed. At a critical  $\lambda = \lambda_c$ , the walls become thermodynamically unstable and the director experiences periodic oscillations about  $\phi = 0$ , which diminish in amplitude with increasing  $\lambda$ .

### III. WAVES IN CHOLESTERIC STRUCTURES

The usual wave equation in linear media for magnetic fields harmonically varying as  $\mathbf{H}(\mathbf{r}, t) = \mathbf{H}(\mathbf{r}) e^{i\omega t}$  is

$$\nabla \times [\underline{\underline{\epsilon}}^{-1}(\mathbf{r})(\nabla \times \mathbf{H})] = \frac{\omega^2}{c^2} \mathbf{H}. \quad (7)$$

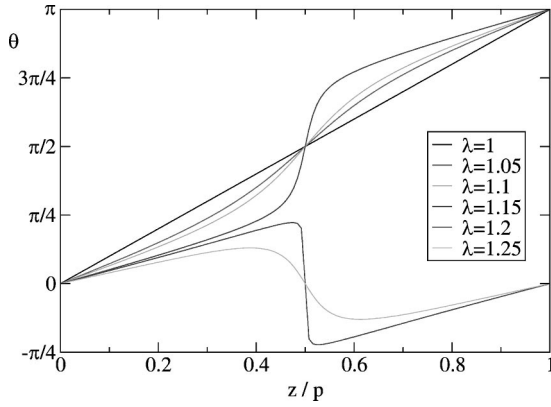


FIG. 3. Dependence of the orientation of the director on distance along the pitch axis for helices subjected to several different  $x$  strains of magnitude  $\lambda$ . Notice the qualitative change in behavior as  $\lambda$  crosses through  $\lambda_c \approx 1.19$ .

The spatial dependence of the inverse dielectric tensor and its control of polarization since it is not spherical is at the heart of our problem. Induced changes in the spatial dependence give the varying band structure.

We expect most cholesteric liquid crystals to be locally uniaxial with one optical axis along the director field  $\mathbf{n}(\mathbf{r})$ . Of course, in general, cholesteric liquid crystals must be locally biaxial since there exist, at a point, three distinct axes (the director with  $\epsilon_{\parallel}$ , the helix axis with  $\epsilon_3$ , and the perpendicular direction with  $\epsilon_{\perp}$ ), but theoretical considerations [28] and studies of oblique incidence by Berreman and Scheffer [10] strongly suggest that  $\epsilon_3 = \epsilon_{\perp}$  to one part in  $(q_0 a)^2 \approx 10^{-4}$ , where  $a$  is the molecular dimension of liquid-crystal subunits. In fact as part of this study Berreman and Scheffer [10] were the first to calculate the band properties of cholesterics away from normal incidence. They took one particular oblique angle ( $45^\circ$ ), rather than the general case that we shall present. A more general study of the oblique structure of undistorted cholesteric liquids is that of Dreher and Meier [29].

As a result, we can write the dielectric tensor in the form  $\epsilon_{ij} = (\epsilon_{\parallel} - \epsilon_{\perp})n_i n_j + \epsilon_{\perp} \delta_{ij}$ , where  $\epsilon_{\parallel}$  is the dielectric constant along the long axis of the nematic mesogen and  $\epsilon_{\perp}$ , is the dielectric constant in any direction perpendicular to the director; see Fig. 1. Likewise the inverse tensor is  $\epsilon_{ij}^{-1} = (1/\epsilon_{\parallel} - 1/\epsilon_{\perp})n_i n_j + 1/\epsilon_{\perp} \delta_{ij}$ . If we rotate to the laboratory frame that is not based upon  $\hat{\mathbf{n}}$ , then this second-rank tensor transforms in the usual way, that is, as a function of  $2\phi$ ,

$$\underline{\underline{\epsilon}}^{-1} = b \left[ \underline{\underline{\delta}} - \alpha \begin{pmatrix} \cos 2\phi & \sin 2\phi & 0 \\ \sin 2\phi & -\cos 2\phi & 0 \\ 0 & 0 & -1 \end{pmatrix} \right], \quad (8)$$

where  $\alpha = (\epsilon_{\parallel} - \epsilon_{\perp}) / (\epsilon_{\parallel} + \epsilon_{\perp})$  and  $b = \frac{1}{2}(1/\epsilon_{\parallel} + 1/\epsilon_{\perp})$ . It is a form reminiscent of  $\underline{\underline{\ell}}^{-1}$  and recognizes that the vectors  $\mathbf{n}$  and  $-\mathbf{n}$  are indistinguishable; in effect the actual period of the liquid crystal is halved.

*Reduction of variables.* We can reduce the wave equation (7) to a dimensionless form by extracting the constant  $b$  from

$\underline{\underline{\epsilon}}^{-1}$  to give  $\underline{\underline{\epsilon}}^{-1} = b \underline{\underline{\tilde{\epsilon}}}^{-1}$  (the tilde denoting a reduced quantity).  $\alpha$  is thus the effective reduced dielectric anisotropy. One reduces lengths by noting simplifications in factors like  $\cos 2\phi = \cos 2qz \rightarrow \cos \tilde{z}$  if  $2qz \rightarrow \tilde{z}$ . Thus a natural choice for reduction of the wave vector is  $\tilde{k} = k/2q$ .

The wave equation becomes

$$\tilde{\nabla} \times [\underline{\underline{\tilde{\epsilon}}}^{-1}(\tilde{z})(\tilde{\nabla} \times \mathbf{H})] = \tilde{\omega}^2 \mathbf{H}. \quad (9)$$

The reduced frequency is  $\tilde{\omega} = \omega/2cq\sqrt{b}$ . Thus the affine contraction of space, as  $\lambda^{-2/7}$ , enters the reduction to  $\tilde{z}$  and also into the frequency since  $q = q_0 \lambda^{2/7}$ . These shifts towards the violet and the contraction of the Brillouin zone should be recalled when examining the band structures that will be presented in reduced form.

de Vries first solved the electric-field equivalent of Eq. (7) for normally incident light,  $(\omega/c)^2 \mathbf{D} = -\partial^2 \mathbf{E} / \partial z^2$ , by transforming  $\mathbf{E}(z)$  into a coordinate frame rotating spatially with the dielectric tensor, so that the matrix connecting  $\mathbf{D}$  with  $\mathbf{E}$  is diagonal [6]. For this reason it was simpler to examine the electric- rather than magnetic-field variation. We first review the classical case in unreduced units. Given that  $\phi = q_0 z$ , in the rotating coordinate system  $(\xi, \eta)$ , the fields are such that

$$\begin{pmatrix} E_x \\ E_y \end{pmatrix} = \begin{pmatrix} \cos(qz) & -\sin(qz) \\ \sin(qz) & \cos(qz) \end{pmatrix} \begin{pmatrix} E_{\xi} \\ E_{\eta} \end{pmatrix} \quad (10)$$

with the simple connection between  $D$  and  $E$ ,

$$\begin{aligned} D_{\xi} &= \epsilon_{\parallel} E_{\xi}, \\ D_{\eta} &= \epsilon_{\perp} E_{\eta}. \end{aligned} \quad (11)$$

Substituting transformation (10) into the electric wave equation, we obtain the eigenlike equation

$$\left(\frac{\omega}{c}\right)^2 \begin{pmatrix} \epsilon_{\parallel} E_{\xi} \\ \epsilon_{\perp} E_{\eta} \end{pmatrix} = - \begin{pmatrix} \partial_z^2 - q^2 & -2q\partial_z \\ 2q\partial_z & \partial_z^2 - q^2 \end{pmatrix} \begin{pmatrix} E_{\xi} \\ E_{\eta} \end{pmatrix}. \quad (12)$$

In this spatially rotating coordinate system, even a state with  $\partial_z E_{\xi} = 0$  and  $\partial_z E_{\eta} = 0$  has a nonzero energy  $\omega = cq$ , arising from the variations in  $\mathbf{B}$  and  $\mathbf{E}$  associated with the frame rotation. For a simply rotating system, Eq. (12) has constant coefficients so that both components are described by a single plane wave of the form  $\mathbf{E} \sim \exp[i(kz - \omega t)]$ . In the rotating frame,  $k=0$  corresponds to solutions at the normal-incidence band edges—these solutions are perfectly in phase with the material rotation. The generic solution has elliptical polarization, parametrized by

$$(E_{\xi}, E_{\eta}) = (A, iB) \exp[i(kz - \omega t)], \quad (13)$$

which in Eq. (12) yields the  $2 \times 2$  matrix equation

$$\begin{pmatrix} \epsilon_{\parallel} \left( \frac{\omega}{c} \right)^2 - q^2 - k^2 & -2iqk \\ -2iqk & \epsilon_{\perp} \left( \frac{\omega}{c} \right)^2 - q^2 - k^2 \end{pmatrix} \begin{pmatrix} A \\ iB \end{pmatrix} = \begin{pmatrix} 0 \\ 0 \end{pmatrix}. \quad (14)$$

In reduced variables, the eigenequation (14) is

$$\begin{pmatrix} \frac{4}{1-\alpha} \tilde{\omega}^2 - 4\tilde{k}^2 - 1 & -4i\tilde{k} \\ 4i\tilde{k} & \frac{4}{1+\alpha} \tilde{\omega}^2 - 4\tilde{k}^2 - 1 \end{pmatrix} \begin{pmatrix} A \\ iB \end{pmatrix} = \begin{pmatrix} 0 \\ 0 \end{pmatrix}, \quad (15)$$

which yields the solutions

$$\lambda = -1 - 4\tilde{k}^2 + \frac{4\alpha\tilde{\omega}^2 \pm \sqrt{(1-\alpha^2)^2\tilde{k}^2 + \alpha^2\tilde{\omega}^4}}{1-\alpha^2}, \quad (16)$$

$$\frac{A}{B} = \frac{\alpha\tilde{\omega}^2 \pm \sqrt{\tilde{k}^2(1-\alpha^2)^2 + \alpha^2\tilde{\omega}^4}}{\tilde{k}(1-\alpha^2)}. \quad (17)$$

Setting  $\lambda=0$  yields the dispersion relation

$$\tilde{\omega} = \pm \frac{1}{2} \sqrt{1 + 4\tilde{k}^2 \pm [16\alpha^2\tilde{k}^4 + 8(2-\alpha^2)\tilde{k}^2 + \alpha^2]^{1/2}}. \quad (18)$$

It is evident that there is one gap in the dispersion relation when  $\tilde{k}=0$  with eigenstates corresponding to the coherent superposition of two plane waves with wave vectors of  $\pm 1/2$  in reduced units [28]. Equation (18) also implies that the lower branch will have a reduced frequency  $\tilde{\omega}_l = \frac{1}{2}\sqrt{1-\alpha}$  and  $B/A=0$ , while the upper branch will have a reduced frequency  $\tilde{\omega}_u = \frac{1}{2}\sqrt{1+\alpha}$  and  $A/B=0$ . Both eigenmodes at the band edge are thus standing circularly polarized waves, the resulting plane of linear polarization (in an infinite sample) rotating with the cholesteric structure. The lower branch points wholly along the rotating  $\xi$  axis, that is, along the director and thus with a higher effective dielectric constant  $1/(1-\alpha)$  in reduced units, while the upper branch points along the rotating  $\eta$  axis, that is, perpendicular to the director and thus with an effective dielectric constant  $1/(1+\alpha)$ . Between them is a range of forbidden frequencies—the band gap. This is most clearly discussed by Kopp and Genack [30]. In the degenerate perturbation analysis for gap scaling in distorted cholesterics of Sec. V B 1 we discuss why simple cholesterics only have one gap.

These solutions inside the cholesteric translate into left- and right-handed circularly polarized light outside the cholesteric. The eigenstate that is split by a band gap is clearly the one that rotates in the same direction of the helix. That is why cholesterics are observed to reflect light with one sense of circular polarization, while light polarized with the opposite circular polarization is transmitted unaffected.

With imposed fields, e.g., electric, magnetic, or mechanical, the simple linear relationship between  $\phi$  and  $z$  is lost. Now, transformation into a set of coordinates rotating with an arbitrary  $\phi = \phi(z)$  yields

$$\begin{pmatrix} E_x \\ E_y \end{pmatrix} = \begin{pmatrix} \cos \phi & -\sin \phi \\ \sin \phi & \cos \phi \end{pmatrix} \begin{pmatrix} E_{\xi} \\ E_{\eta} \end{pmatrix}. \quad (19)$$

We can then insert this expression into the electric wave equation and use Eqs. (11) to obtain instead of Eq. (12) the relation

$$\left( \frac{\omega}{c} \right)^2 \begin{pmatrix} \epsilon_{\parallel} E_{\xi} \\ \epsilon_{\perp} E_{\eta} \end{pmatrix} = \begin{pmatrix} \phi'^2 - \partial_z^2 & 2\phi' \partial_z + \phi'' \\ -2\phi' \partial_z - \phi'' & \phi'^2 - \partial_z^2 \end{pmatrix} \begin{pmatrix} E_{\xi} \\ E_{\eta} \end{pmatrix}. \quad (20)$$

In general  $\phi'$  and  $\phi''$  are nontrivial functions of  $z$ , see Figs. 2 and 3, and de Vries's approach in Eq. (20) fails to give analytical results. In the following section we develop a band-structure alternative of greater applicability.

#### IV. CHOLESTERIC PHOTONIC BAND STRUCTURE

The technique we use below was introduced by Ho, Chan, and Soukoulis [31] for the case of scalar dielectric constants. They Fourier transformed the dielectric constant and then inverted it. A refinement of Meade and co-workers [32] reversed the order of these processes; we follow this route. The subtleties of relative rates of convergence in the two cases are further discussed by Busch and John [22], who also consider the tensor dielectric constant case that we follow below. The above authors were concerned with calculating the properties of light propagating through an only piecewise continuous dielectric medium: their photonic media typically consist of periodic inclusions of different dielectric constants. By contrast we are concerned with continuous media, the periodic rotation of the tensor dielectric constant leading to more subtle effects. We do not find the convergence difficulties introduced by the spatial discontinuities in the systems of the above authors. A related, highly tensorial band-structural problem is that of the liquid-crystal blue phases with, in some sense, a helical cholesteric variation in three dimensions; see, for instance, Hornreich *et al.* [33].

Using Bloch's theorem, the solutions to Eq. (7) can be expanded as

$$\mathbf{H}(\mathbf{r}) = \sum_{\mathbf{G}} \mathbf{h}_{\mathbf{G}} e^{i(\mathbf{k}+\mathbf{G}) \cdot \mathbf{r}}, \quad (21)$$

where  $\{\mathbf{G}\}$  is the set of all reciprocal lattice vectors (with  $e^{i\mathbf{G} \cdot \mathbf{T}} = 1$ ).

Since  $\mathbf{H}$  is transverse, we can pick two unit basis vectors  $\hat{e}_{(\mathbf{G}\gamma)}$  for each  $\mathbf{G}$  such that

$$\nabla \cdot (\mathbf{G}\gamma) \quad [\hat{e}_{(\mathbf{G}\gamma)} \cdot (\mathbf{k} + \mathbf{G})] = 0, \quad (22)$$

$$\nabla \cdot (\mathbf{G}\gamma\gamma') \quad [\hat{e}_{(\mathbf{G}\gamma)} \cdot \hat{e}_{(\mathbf{G}\gamma')}] = \delta_{\gamma,\gamma'}. \quad (23)$$

Thus  $\mathbf{k} + \mathbf{G}$  and  $\hat{e}_{(\mathbf{G}\gamma)}$  form an orthogonal triad of vectors in space for each  $\mathbf{G}$ , and  $\hat{e}_{(\mathbf{G}\gamma)}$  may be different for each  $\mathbf{G}$ , in general. Each plane-wave component of  $\mathbf{H}$  is thus guaranteed to point to the plane created by the  $\hat{e}_{(\mathbf{G}\gamma)}$ . This gives the Fourier representation of the  $\mathbf{H}$  field (21),

$$\mathbf{H}(\mathbf{r}) = \sum_{\mathbf{G}} \sum_{\gamma=1}^2 h_{(\mathbf{G}\gamma)} \hat{e}_{(\mathbf{G}\gamma)} e^{i(\mathbf{k} + \mathbf{G}) \cdot \mathbf{r}}. \quad (24)$$

We also expand  $\underline{\epsilon}^{-1}$  in a plane-wave basis,

$$\underline{\epsilon}^{-1}(\mathbf{r}) = \sum_{\mathbf{G}'} \underline{\epsilon}_{\mathbf{G}'}^{-1} e^{i\mathbf{G}' \cdot \mathbf{r}}. \quad (25)$$

Substituting Eqs. (24) and (25) into Eq. (7) gives

$$\begin{aligned} & \left(\frac{\omega}{c}\right)^2 \sum_{\mathbf{G}} \sum_{\gamma=1}^2 \hat{e}_{(\mathbf{G}\gamma)} h_{(\mathbf{G}\gamma)} e^{i(\mathbf{k} + \mathbf{G}) \cdot \mathbf{r}} \\ &= - \sum_{\mathbf{G}, \mathbf{G}'} \sum_{\gamma=1}^2 h_{(\mathbf{G}\gamma)} (\mathbf{k} + \mathbf{G} + \mathbf{G}') \\ & \quad \times \{ \underline{\epsilon}_{\mathbf{G}' - \mathbf{G}}^{-1} [(\mathbf{k} + \mathbf{G}) \hat{e}_{(\mathbf{G}\gamma)}] \} \exp[i(\mathbf{k} + \mathbf{G} + \mathbf{G}') \cdot \mathbf{r}]. \quad (26) \end{aligned}$$

Transforming  $\mathbf{G}' \rightarrow \mathbf{G}' - \mathbf{G}$ , multiplying by  $e^{-i(\mathbf{k} + \mathbf{G}_0) \cdot \mathbf{r}}$  and integrating over the unit cell gives

$$\begin{aligned} & \left(\frac{\omega}{c}\right)^2 \sum_{\gamma} h_{(\mathbf{G}'\gamma)} \hat{e}_{(\mathbf{G}'\gamma)} = - \sum_{\mathbf{G}} \sum_{\gamma} h_{(\mathbf{G}\gamma)} (\mathbf{k} + \mathbf{G}') \\ & \quad \times \{ \underline{\epsilon}_{\mathbf{G}' - \mathbf{G}}^{-1} [(\mathbf{k} + \mathbf{G}) \times \hat{e}_{(\mathbf{G}\gamma)}] \}. \quad (27) \end{aligned}$$

If we multiply Eq. (27) by  $\hat{e}_{(\mathbf{G}\gamma)'}$  and assume without loss of generality that

$$(\mathbf{k} + \mathbf{G}) \times \hat{e}_{(\mathbf{G}1)} = \hat{e}_{(\mathbf{G}2)} \quad \text{and} \quad (\mathbf{k} + \mathbf{G}) \times \hat{e}_{(\mathbf{G}2)} = -\hat{e}_{(\mathbf{G}1)}, \quad (28)$$

we obtain

$$\begin{aligned} & \left(\frac{\omega}{c}\right)^2 h_{(\mathbf{G}\gamma)'} = -|\mathbf{k} + \mathbf{G}| \sum_{\mathbf{G}} h_{(\mathbf{G}1)} \hat{e}_{(\mathbf{G}\gamma)'} \cdot [(\mathbf{k} + \mathbf{G}') \\ & \quad \times (\underline{\epsilon}_{\mathbf{G}' - \mathbf{G}}^{-1} \cdot \hat{e}_{(\mathbf{G}2)})] - h_{(\mathbf{G}2)} \hat{e}_{(\mathbf{G}\gamma)'} \cdot [(\mathbf{k} + \mathbf{G}') \\ & \quad \times (\underline{\epsilon}_{\mathbf{G}' - \mathbf{G}}^{-1} \cdot \hat{e}_{(\mathbf{G}1)})]. \quad (29) \end{aligned}$$

In Eq. (29) the  $h_{(\mathbf{G}\gamma)}$  are linked across  $\mathbf{G}$  and  $\gamma$  spaces. Defining a doublet

$$\mathbf{h}_{\mathbf{G}} = \begin{pmatrix} h_{(\mathbf{G}1)} \\ h_{(\mathbf{G}2)} \end{pmatrix},$$

Eq. (29) becomes a matrix equation

$$\left(\frac{\omega}{c}\right)^2 \mathbf{h}_{\mathbf{G}'} = \sum_{\mathbf{G}} \underline{A}_{\mathbf{G}'\mathbf{G}} \mathbf{h}_{\mathbf{G}}, \quad (30)$$

where  $\underline{A}_{\mathbf{G}'\mathbf{G}}$  is given by

$$\underline{A}_{\mathbf{G}'\mathbf{G}} = -|\mathbf{k} + \mathbf{G}| \begin{pmatrix} \hat{e}_{(\mathbf{G}'1)} \cdot [(\mathbf{k} + \mathbf{G}') \times (\underline{\epsilon}_{\mathbf{G}' - \mathbf{G}}^{-1} \cdot \hat{e}_{(\mathbf{G}2)})] & -\hat{e}_{(\mathbf{G}'1)} \cdot [(\mathbf{k} + \mathbf{G}') \times (\underline{\epsilon}_{\mathbf{G}' - \mathbf{G}}^{-1} \cdot \hat{e}_{(\mathbf{G}1)})] \\ \hat{e}_{(\mathbf{G}'2)} \cdot [(\mathbf{k} + \mathbf{G}') \times (\underline{\epsilon}_{\mathbf{G}' - \mathbf{G}}^{-1} \cdot \hat{e}_{(\mathbf{G}2)})] & -\hat{e}_{(\mathbf{G}'2)} \cdot [(\mathbf{k} + \mathbf{G}') \times (\underline{\epsilon}_{\mathbf{G}' - \mathbf{G}}^{-1} \cdot \hat{e}_{(\mathbf{G}1)})] \end{pmatrix}. \quad (31)$$

For 1D structures periodic along  $z$ , the reciprocal lattice vectors  $\mathbf{G}$  are  $G = 2nq\hat{z}$ ,  $n$  being an integer. We now consider specific cases of increasing complexity.

### A. Normal incidence

It is clear that the two unit vectors  $\hat{e}_{(\mathbf{G}\gamma)}$  are in the  $xy$  plane. Choose without loss of generality  $\forall_{\mathbf{G}} \hat{e}_{(\mathbf{G}1)} = \hat{x}$  and  $\forall_{\mathbf{G}} \hat{e}_{(\mathbf{G}2)} = \hat{y}$ . In this case, it is obvious from Eq. (31) that the  $z$  components of the reduced inverse dielectric tensor  $\underline{\epsilon}^{-1}$  can be suppressed (the tilde is also suppressed), which allows one to write

$$\underline{\epsilon}_{\mathbf{G}' - \mathbf{G}}^{-1} = \begin{pmatrix} (\underline{\epsilon}_{\mathbf{G}' - \mathbf{G}}^{-1})_{xx} & (\underline{\epsilon}_{\mathbf{G}' - \mathbf{G}}^{-1})_{xy} \\ (\underline{\epsilon}_{\mathbf{G}' - \mathbf{G}}^{-1})_{yx} & (\underline{\epsilon}_{\mathbf{G}' - \mathbf{G}}^{-1})_{yy} \end{pmatrix}. \quad (32)$$

From Eq. (31) the matrix  $\underline{A}_{\mathbf{G}'\mathbf{G}}$  becomes

$$\underline{A}_{\mathbf{G}'\mathbf{G}} = |\mathbf{k} + \mathbf{G}| |\mathbf{k} + \mathbf{G}'| \begin{pmatrix} (\underline{\epsilon}_{\mathbf{G}' - \mathbf{G}}^{-1})_{yy} & -(\underline{\epsilon}_{\mathbf{G}' - \mathbf{G}}^{-1})_{yx} \\ -(\underline{\epsilon}_{\mathbf{G}' - \mathbf{G}}^{-1})_{xy} & (\underline{\epsilon}_{\mathbf{G}' - \mathbf{G}}^{-1})_{xx} \end{pmatrix}. \quad (33)$$

From Eq. (8) the Fourier components of the reduced inverse dielectric tensor become

$$\underline{\epsilon}_{\mathbf{G}' - \mathbf{G}}^{-1} = \begin{pmatrix} \delta_{\mathbf{G}\mathbf{G}'} - \alpha c_{\mathbf{G}' - \mathbf{G}} & -\alpha s_{\mathbf{G}' - \mathbf{G}} & 0 \\ -\alpha s_{\mathbf{G}' - \mathbf{G}} & \delta_{\mathbf{G}\mathbf{G}'} + \alpha c_{\mathbf{G}' - \mathbf{G}} & 0 \\ 0 & 0 & (1 + \alpha) \delta_{\mathbf{G}\mathbf{G}'} \end{pmatrix}, \quad (34)$$

where

$$c_{\mathbf{G}} = \int_{\text{unit cell}} d\mathbf{r} e^{-i\mathbf{G}\cdot\mathbf{r}} \cos 2\phi, \quad (35)$$

$$s_{\mathbf{G}} = \int_{\text{unit cell}} d\mathbf{r} e^{-i\mathbf{G}\cdot\mathbf{r}} \sin 2\phi. \quad (36)$$

If the first reciprocal lattice vector is  $\mathbf{G}_1$ , then uniform helical advancement ( $\phi = q_0 z$ ) gives  $c_{\pm\mathbf{G}_1} = 1/2$ ,  $\mathbf{V}_{\mathbf{G}\neq\pm\mathbf{G}_1} c_{\mathbf{G}} = 0$ ,  $s_{\pm\mathbf{G}_1} = \mp 1/2$ , and  $\mathbf{V}_{\mathbf{G}\neq\pm\mathbf{G}_1} s_{\mathbf{G}} = 0$ . With distortions and, therefore, harmonics, more of the  $c_{\mathbf{G}}$  and the  $s_{\mathbf{G}}$  will be important.

Given this definite form for  $\underline{\epsilon}_{\mathbf{G}'-\mathbf{G}}^{-1}$ , we can substitute into Eq. (33) to find that for normal incidence

$$\underline{A}_{\mathbf{G}',\mathbf{G}} = |\mathbf{k} + \mathbf{G}| |\mathbf{k} + \mathbf{G}'| \times \begin{pmatrix} \delta_{\mathbf{G},\mathbf{G}'} + \alpha c_{\mathbf{G}'-\mathbf{G}} & \alpha s_{\mathbf{G}'-\mathbf{G}} \\ \alpha s_{\mathbf{G}'-\mathbf{G}} & \delta_{\mathbf{G},\mathbf{G}'} - \alpha c_{\mathbf{G}'-\mathbf{G}} \end{pmatrix}. \quad (37)$$

Equation (37) should be rewritten in a fully dimensionless form.  $\mathbf{G}$  points along  $\hat{z}$  and for normal incidence  $\mathbf{k}$  does too. Thus  $|\mathbf{k} + \mathbf{G}| = k + G$  simply. Recall that  $G = 2nq\hat{z}$ ,  $n$  being an integer, and using the previous definitions for  $\tilde{k}$  and  $\tilde{\omega}$ , one obtains the matrix form of the reduced wave equation,

$$\tilde{\omega}^2 \mathbf{h}_n = (\tilde{k} + n') \sum_n (\tilde{k} + n) \times \begin{pmatrix} \delta_{nn'} + \alpha c_{n'-n} & \alpha s_{n'-n} \\ \alpha s_{n'-n} & \delta_{nn'} - \alpha c_{n'-n} \end{pmatrix} \mathbf{h}_n. \quad (38)$$

### B. Oblique incidence

We now allow  $\mathbf{k}$  to point in any direction. Cholesterics, when coarse grained, have cylindrical symmetry. Thus, the optical properties will be the same, to within the same phase, for any combination of  $k_x$  and  $k_y$  with the same overall magnitude  $k_\rho = \sqrt{k_x^2 + k_y^2}$ . Thus, without loss of generality,  $\mathbf{k} = k_\rho \hat{\rho} + k_z \hat{z}$  in cylindrical coordinates. Thus from Bloch's theorem, one writes  $\mathbf{H}$  as a product of plane waves along  $\hat{\rho}$ , and  $\hat{z}$  times a function periodic in  $z$ , and Eq. (24) takes the form

$$\mathbf{H}(\mathbf{r}) = \sum_G \sum_{\gamma=1}^2 h_{(G\gamma)} \hat{e}_{(G\gamma)} \exp\{i[k_\rho \rho + (k_z + G)z]\}. \quad (39)$$

We can easily show that

$$\nabla \cdot \mathbf{H}(\mathbf{r}) = i \sum_G \sum_{\gamma=1}^2 h_{(G\gamma)} [k_\rho \hat{\rho} + (k_z + G) \hat{z}] \cdot \hat{e}_{(G\gamma)} \times \exp\{i[k_\rho \rho + (k_z + G)z]\} \quad (40)$$

and enforce the transversality constraint  $\nabla \cdot \mathbf{H} = 0$  by requiring individual components of Eq. (40) to be transverse. Since components are linearly independent, this is also the most general way available to ensure transversality. Then the particular form of  $\mathbf{k}$  allows us to write Eq. (22) as

$$\mathbf{V}_{G,\gamma} [k_\rho \hat{\rho} + (k_z + G) \hat{z}] \cdot \hat{e}_{(G\gamma)} = 0. \quad (41)$$

This condition puts two constraints on the coefficients of  $\{\hat{e}_{(G\gamma)}\}$  for a given  $G$ . There is one constraint for each  $\gamma$  imposed by the requirement that each  $\hat{e}_{(G\gamma)}$  is a unit vector, and one more constraint from the orthogonality requirement given by Eq. (23). Thus, there are a total of five constraints and six components of  $\hat{e}_{(G\gamma)}$  for each  $G$ , allowing us to choose one of the components arbitrarily. The simplest choice is to set  $\hat{e}_{(G1)} = \hat{\theta}$ , where  $\hat{\theta}$  is the unit vector in the  $xy$  plane orthogonal to  $\hat{\rho}$ . This choice trivially satisfies the orthogonality condition (41). We then obtain for the direction of  $\hat{e}_{(G2)}$ ,

$$\hat{e}_{(G2)} = \frac{1}{\sqrt{k_\rho^2 + (k_z + G)^2}} [(k_z + G) \hat{\rho} - k_\rho \hat{z}] \quad (42)$$

(which is unique to within a factor of  $\pm 1$ ). Most importantly, we observe that unlike what we saw for normal incidence, each  $\hat{e}_{(G\gamma)}$  will be different for each  $G$ , in general.

We can find a solution for  $\underline{A}_{n',n}$  in the reduced form

$$\tilde{\omega}^2 \mathbf{h}_n = \sum_n \underline{A}_{n',n} \mathbf{h}_n, \quad (43)$$

which is equivalent to Eq. (30) in a dimensionless form. For simplicity, we calculate  $\underline{A}$  in Cartesian coordinates. Thus  $\mathbf{h}_n$  must also be in Cartesian coordinates, and we are obliged to express  $\tilde{\mathbf{k}} = \tilde{k}_\rho \hat{y} + \tilde{k}_z \hat{z}$ . The result is

$$\underline{A}_{n',n} = \begin{pmatrix} (\tilde{k}_z + n)(\tilde{k}_z + n')(\delta_{nn'} + \alpha c_{n'-n}) + \tilde{k}_\rho^2(1 + \alpha) \delta_{nn'} & (\tilde{k}_z + n)(\tilde{k}_z + n') \alpha s_{n'-n} & -\tilde{k}_\rho(\tilde{k}_z + n') \alpha s_{n'-n} \\ \alpha(\tilde{k}_z + n)(\tilde{k}_z + n') s_{n'-n} & (\tilde{k}_z + n)(\tilde{k}_z + n')(\delta_{nn'} - \alpha c_{n'-n}) & -\tilde{k}_\rho(\tilde{k}_z + n')(\delta_{nn'} - \alpha c_{n'-n}) \\ -\tilde{k}_\rho(\tilde{k}_z + n) \alpha s_{n'-n} & -\tilde{k}_\rho(\tilde{k}_z + n)(\delta_{nn'} - \alpha c_{n'-n}) & \tilde{k}_\rho^2(\delta_{nn'} - \alpha c_{n'-n}) \end{pmatrix}. \quad (44)$$

However, since  $\mathbf{H}(\mathbf{r})$  must be transverse, we know that it really only has two degrees of freedom for each  $G$ , i.e., an  $h_{(G1)}$  and an  $h_{(G2)}$ , i.e.,  $h_{(Gx)}$ ,  $h_{(Gy)}$ , and  $h_{(Gz)}$  are interdependent. This implies that we can transform  $\underline{\underline{A}}'_{n',n}$  into a  $2 \times 2$  matrix, which we denote as  $\underline{\underline{A}}'_{n',n}$ , so that the solution for the analog of Eq. (43) is

$$\tilde{\omega}^2 \mathbf{h}'_n = \sum_n \underline{\underline{A}}'_{n',n} \mathbf{h}'_n, \quad (45)$$

where the doublet

$$\mathbf{h}'_n = \begin{pmatrix} h_{(n1)} \\ h_{(n2)} \end{pmatrix}.$$

The resulting expression for  $\underline{\underline{A}}'$  is

$$\underline{\underline{A}}'_{n',n} = \begin{pmatrix} (\tilde{k}_z + n)(\tilde{k}_z + n')(\delta_{nn'} + \alpha c_{n'-n}) + \tilde{k}_\rho^2(1 + \alpha)\delta_{nn'} & \alpha(\tilde{k}_z + n)(\tilde{k}_z + n') \sqrt{1 + \left(\frac{\tilde{k}_\rho}{\tilde{k}_z + n}\right)^2} s_{n'-n} \\ \alpha(\tilde{k}_z + n)(\tilde{k}_z + n') \sqrt{1 + \left(\frac{\tilde{k}_\rho}{\tilde{k}_z + n'}\right)^2} s_{n'-n} & (\tilde{k}_z + n)(\tilde{k}_z + n')(\delta_{nn'} + \alpha c_{n'-n}) \sqrt{1 + \left(\frac{\tilde{k}_\rho}{\tilde{k}_z + n}\right)^2} \sqrt{1 + \left(\frac{\tilde{k}_\rho}{\tilde{k}_z + n'}\right)^2} \end{pmatrix}. \quad (46)$$

## V. SOLUTION OF THE BAND STRUCTURES

### A. Method

Solution of Eq. (38) requires a reasonably sized plane-wave basis set. If  $n$  and  $n'$  range from  $N$  to  $-N$ , we have a  $2(2N+1) \times 2(2N+1)$  matrix, which links  $\mathbf{h} = (\dots h_{(-1,1)} h_{(0,1)} h_{(1,1)} \dots h_{(-1,2)} h_{(0,2)} h_{(1,2)} \dots)$  and  $\mathbf{h}'$ , which is defined similarly. We represent this linkage by the eigenvalue equation in the simple form

$$\tilde{\omega}^2 \mathbf{h}' = \underline{\underline{A}} \mathbf{h}, \quad (47)$$

where

$$\underline{\underline{A}} = \begin{pmatrix} \underline{\underline{A}}^{1,1} & \underline{\underline{A}}^{1,2} \\ \underline{\underline{A}}^{2,1} & \underline{\underline{A}}^{2,2} \end{pmatrix}, \quad (48)$$

and each individual  $\underline{\underline{A}}^{\alpha,\beta}$  is an  $(2N+1) \times (2N+1)$  array, calculated from the corresponding components of Eq. (38), e.g.,  $\underline{\underline{A}}^{1,1}_{n',n} = (\tilde{k} + n)(\tilde{k} + n')(\delta_{nn'} + \alpha c_{n'-n})$ . Since  $(\underline{\underline{A}}^{1,1}_{n',n})^* = \underline{\underline{A}}^{1,1}_{n,n'}$ , then  $\underline{\underline{A}}$  is Hermitian by inspection.

To solve the eigenvalue problem, we first construct the  $\underline{\underline{A}}$  matrix, then diagonalize it. The construction of the matrix requires the calculation of the Fourier coefficients, which we do by first calculating the angle of the director for  $2N+1$  evenly spaced values of  $z$  from Eq. (6) and the appropriate trigonometric identities for a fixed  $r$ ,  $\lambda$ , and thus  $\lambda_{yy}$ . Then we populate the matrix using Eqs. (38) and (48) for a given  $\alpha$  and  $\tilde{k}$ . Next, we diagonalize the matrix, using the procedure “zheev” in LAPACK, which computes all the eigenvalues and eigenvectors of a complex, double-precision Hermitian matrix [34].

For piecewise continuous systems the subtleties of convergence can be great [22]. Here we simply double  $N$  and see if there are any differences in the structures we obtain (none could be discerned on doubling our working value of  $N$ ). If

we were to calculate band structures for elastomers close to the critical strain, where the twist walls and hence the spatial rotation of the dielectric tensor are very sharp, we would expect many more Fourier components of the dielectric tensor to arise. From this would come also an increasing importance of the very much higher order stop bands, but experimentally these would then be deep into the ultraviolet which does not interest us particularly. On either side of the critical strain where the director twist is more moderate, there seem to be no convergence problems.

### B. Normal incidence

*Ideal helices.* There are only two Fourier components, whence  $c_n$  and  $s_n$  are simple:  $c_{\pm 1} = 1/2$ ,  $\forall_{|n| \neq 1} c_n = 0$  and  $s_{\pm 1} = \mp i/2$ ,  $\forall_{|n| \neq 1} s_n = 0$ . These sine and cosine components link matrix elements a distance of  $n$  apart. Since they vanish for  $n > 1$ , we need only consider a small ( $N=2$ ) matrix, which we then diagonalize to obtain the system's eigenvalues while stepping through values of  $k$  for half of one Brillouin zone. The results are depicted in Fig. 4. In an extended-zone scheme, there would be two bands associated with each  $k$ , two for each  $k+2q$ , two for each  $k+4q$ , etc. Two bands arise, in general, because photons have two transverse, orthogonal polarizations. We have discussed above the qualitative nature of the eigenstates.

Note that the reduced wave vector  $\tilde{k}$  of the discussion around Eqs. (15)–(18) of the de Vries analysis, henceforth referred to as  $\tilde{k}'$ , is in the spatially rotating coordinate frame, while the  $\tilde{k}$  here is in the stationary lab frame. Qualitatively, a wave with a  $\tilde{k}'$  in the rotating frame is a coherent superposition of two waves with wave vectors  $\tilde{k}' + 1/2$  and  $\tilde{k}' - 1/2$  in the stationary frame. The gap in the dispersion relation that occurs at  $\tilde{k}' = 0$  in the de Vries analysis thus corresponds in a nonrotating frame to a coherent superposition of states with  $\tilde{k} = 1/2$  and  $\tilde{k} = -1/2$ . The two polarizations

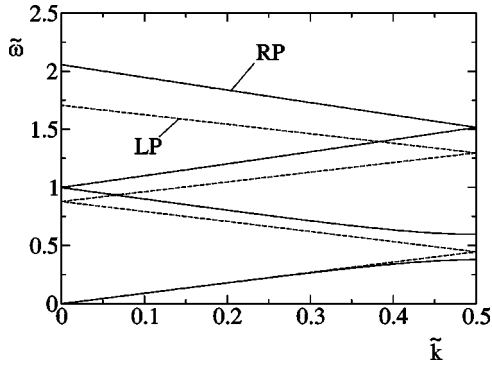


FIG. 4. Dispersion relation at normal incidence from band-structure calculations ( $\tilde{\omega}$  versus  $\tilde{k}$ ) for an ideal helix, with  $\alpha = 0.18$ . There is one gap for one polarization, at  $\tilde{k} = 1$ , and no gap for the other polarization.

have distinctive behaviors—one eigenstate has one gap at the first Brillouin-zone boundary, while the other has no such gap. Also there are no gaps for higher-order reflections. The absence of higher-order gaps does not hold, in general, but only for normal incidence.

*Distorted helices.* We choose a (fixed) representative value for the mechanical anisotropy  $r$  and values of  $\lambda$ . We numerically minimize the coarse-grained energy  $F(\lambda, \lambda_{yy}, r)$  with respect to  $\lambda_{yy}$  to obtain its value. Trigonometric identities can be used to obtain the corresponding values of  $\cos 2\phi$  and  $\sin 2\phi$  from  $\tan 2\phi$  in Eq. (6). A fast Fourier transform yields values of  $c_n$  and  $s_n$ .

Given values of  $s_n$  and  $c_n$  at a given  $\lambda$ , we can calculate the band structure numerically corresponding to this deformation. We illustrate two examples:  $\lambda = 1.1 < \lambda_c$  in Fig. 5 and  $\lambda = 1.3 > \lambda_c$  in Fig. 6, both for a network with  $r = 1.9$ . In Fig. 5, the sample is stretched by less than the critical strain, which is given by  $\lambda_c \approx r^{2/7} \approx 1.19$  [26,27]. Stretching leads to coarsening of the helix, which in turn gives rise to more gaps at higher orders at the Brillouin-zone boundaries, particularly for the polarization that rotates along with the helix. But there are also smaller gaps that arise for the opposite handedness even before we reach the critical strain  $e_c$ . We can explain this phenomenon by considering that, in the uniformly rotating frame in which our original  $E_\xi$  and  $E_\eta$  live, there are, in effect, rotations of  $\mathbf{n}$  both forwards and backwards that arise from deviations of  $\phi'(z)$  from the unperturbed constant value of  $q_0$  (see Figs. 2 and 3). The size and scaling of these gaps is discussed below. The position of these gaps is constant to the first order in reduced units, but actually varies in a physical system. In particular, since a uniaxial strain of  $\lambda$  along  $x$  leads to a contraction  $\lambda_{zz} = \lambda^{-2/7}$ , the wave vector  $q = q_0 \lambda^{2/7}$  currently reducing physical wave vectors is increasing. Since the Brillouin-zone boundaries occur at integer multiples of  $q$ , they will thus shift to higher values. Physically, that will correspond to reflections at higher frequencies. Since  $\tilde{\omega} = \omega/2cq\sqrt{b}$ , a constant  $\tilde{\omega}$  corresponds to a physical  $\omega$  that also scales like  $\omega = \omega_0 \lambda^{2/7}$ , where  $\omega_0$  denotes a frequency of interest at zero strain. Thus, these shifts are scaled away in Figs. 5 and 6. Experimental evidence for the predicted shift in the 1D band

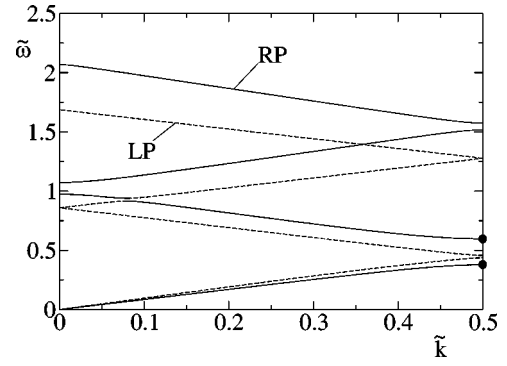


FIG. 5. Band structure for a cholesteric elastomer at a deformation of  $\lambda = 1.1$ , with anisotropy  $r = 1.9$ . The single stop band of the ideal helix evolves into that indicated by the dots.

gaps toward the ultraviolet has been seen in two sets of experiments. First, there is a change in the color of cholesteric monodomain rubbers upon stretching [20,35]. Furthermore, there are changes in the color of the lasing mode as stretching proceeds [19].

In Fig. 6, the sample is stretched beyond the critical strain. This gives rise to a qualitative change in the behavior of the director  $\phi(z)$  (see Fig. 3), and thus a qualitative change in the band structure. The most important effect is the elimination of the persistent bias toward rotation in one direction present at smaller strains; now, the director rotates periodically, swinging almost equally in both directions. Removing this bias means that there should be little difference between the optical properties of left- and right-circularly polarized light. Furthermore, the magnitude of this difference will decrease with increasing  $e$ . As a result, the circular dichroism of the material should disappear, and the eigenmodes of light inside the stretched cholesteric medium should be linearly polarized. Also, we note that the scaling behavior of  $\lambda_{zz}$  crosses over from the nonclassical  $\lambda^{-2/7}$  response to a  $\lambda^{-1/2}$  response, the classical exponent predicted for isotropic elastomers (e.g., rubbers without nematic ordering). That in turn implies that the frequencies reflected increase more quickly with strain, i.e.,  $\omega = \omega_0 \lambda^{1/2}$ , but the range decreases in width, owing to the decreasing magnitude of the oscillations about  $\phi = 0$ .

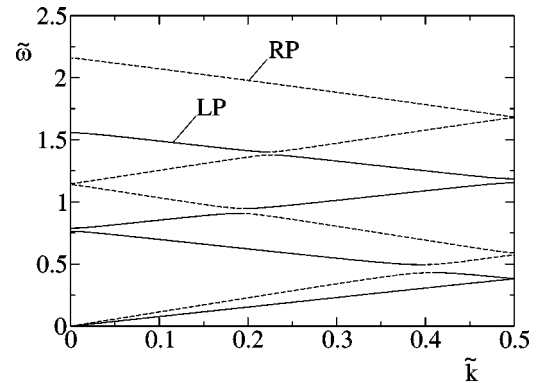


FIG. 6. Band structure for a cholesteric elastomer at a deformation of  $\lambda = 1.3$ , with anisotropy  $r = 1.9$ .

### Perturbation theory of gap scaling at normal incidence

A case where semianalytical perturbative understanding can be gained is that of small deviations from ideal behavior. For cholesteric elastomers, small deviations from ideality correspond to a moderate  $x$  strain perpendicular to the pitch axis. Perturbation theory shows that small deviations away from ideality lead to small values for  $c_n$  and  $s_n$ , where  $|n| \neq 1$ . We expect these small values to scale as power laws in the small parameter of the problem, the elastic strain  $e \equiv \lambda - 1$ . The scaling of these coefficients is given by

$$s_n = \begin{cases} 0 & \text{if } n=0 \\ \mp \frac{i}{2}[1 - O(e^2)] & \text{if } n = \pm 1 \\ \mp iO(e^{n-1}) & \text{otherwise,} \end{cases} \quad (49)$$

$$c_n = \begin{cases} O(e) & \text{if } n=0 \\ \frac{1}{2}[1 - O(e^2)] & \text{if } n = \pm 1 \\ O(e^{n-1}) & \text{otherwise.} \end{cases} \quad (50)$$

The variation of the Fourier components of  $\cos 2\phi(z)$  is illustrated in Fig. 7 for a cholesteric elastomer under an  $x$  strain of  $e$ . The solid lines are the perturbation theoretical results of Eq. (50). Equally precise agreement between perturbation analysis and numerics is found for the Fourier components of  $\sin 2\phi(z)$ .

A similar pattern can be seen in the case of a liquid cholesteric under an external electric or magnetic field, as shown in Fig. 8, with the corresponding Fourier components of  $\sin 2\phi(z)$  also given precisely by the perturbation analysis. We can calculate the scaling behavior for  $c_n$  and  $s_n$  in an external field by transforming the scaling laws given in Eqs. (49) and (50), and effecting the transformation  $e \rightarrow (H/H_c)^2$ , for  $H \leq H_c$ .

We can apply second-order degenerate perturbation theory to calculate the approximate size and scaling of the normal-incidence band gaps. Identifying two degenerate states,  $n$  and  $n'$ , we construct the reduced matrix  $\underline{D}$  with couplings between  $A_{n'n} = A_{nn'}$  between them,

$$\underline{D} = \begin{pmatrix} A_{nn} & A_{nn'} \\ A_{n'n} & A_{n'n'} \end{pmatrix}. \quad (51)$$

For light normally incident upon a distorted cholesteric helix, Eq. (38) gives  $A_{nn} = (\tilde{k} + n)^2(1 + \alpha c_0)$  and  $A_{n'n'} = (\tilde{k} + n')^2(1 - \alpha c_0)$ . The off-diagonal elements are  $A_{n'n} = (A_{nn})^* = \alpha(\tilde{k} + n)(\tilde{k} + n')s_{n'-n}$  (since  $A$  is Hermitian). Since we are interested in splitting between nearly degenerate energy levels,  $A_{nn} \approx A_{n'n'}$ , which is satisfied when  $|\tilde{k} + n| = |\tilde{k} + n'|$ . For the interesting case where  $n \neq n'$ , one has  $\tilde{k} = -(n + n')/2$ . Substituting back into Eq. (51), we obtain

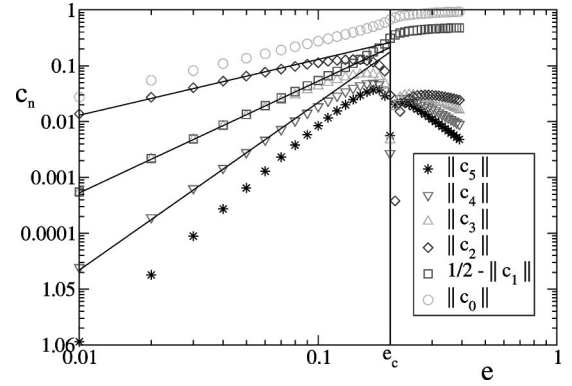


FIG. 7. Dependence of the Fourier coefficients  $c_n$  on uniaxial  $x$  strain  $e$  in a cholesteric elastomer.

$$\underline{D} = \begin{pmatrix} \frac{(n-n')^2}{4}(1 + \alpha c_0) & -\alpha \frac{(n-n')^2}{4}s_{n'-n} \\ -\alpha \frac{(n-n')^2}{4}s_{n-n'} & \frac{(n-n')^2}{4}(1 - \alpha c_0) \end{pmatrix}. \quad (52)$$

From Eq. (52), we obtain a pair of eigenvalues corresponding to the two fresh frequencies resulting from the splitting of the degeneracy. In a dimensionless form, they are given by the expression

$$\tilde{\omega}^2 = \left( \frac{\delta n}{2} \right)^2 [1 \pm \alpha \sqrt{c_0^2 - s_{\delta n}^2}], \quad (53)$$

where  $\delta n = n - n'$ . For an undistorted helix,  $c_0 = 0$ ,  $s_{-1} = -s_1 = i/2$ , and  $\forall_{|n| \neq 1} s_n = 0$ , which gives us the result  $\tilde{\omega}^2 = \frac{1}{4}(1 \pm \frac{1}{2}\alpha)$ , corresponding for small  $\alpha$  to a splitting  $\delta \tilde{\omega} = \alpha/4$ , a linear dependence on the reduced dielectric anisotropy, as originally predicted by de Vries. All other gaps will vanish since  $\forall_{|\delta n| \neq 1} s_{\delta n} = 0$ .

For a slightly distorted helix, given the scaling relations we found before, we can generalize from Eq. (53) to calculate the size of the gap for any order. Given that  $c_0 = 0$ , we obtain  $\delta \tilde{\omega} = (\delta n/2)\alpha |s_{\delta n}|$ . Since we already know how the Fourier coefficients scale with the (small) strain  $e$ , we immediately know how the gaps should behave as well:  $\delta \tilde{\omega} \approx (\delta n/2)\alpha e^{\delta n - 1}$ . These predictions are confirmed qualitatively, however, the results are not exact.

One must be more precise with the polarization vectors of the photons, perhaps analogous to the detail required in spin polarized electronic structure calculations. Physically, this is because the inverse dielectric tensor represents an effective potential for the photons. Deviations of the dielectric tensor from a multiple of the unit tensor represent the magnitude of the difference of the effective potential acting upon different polarizations. Moreover, in our problem the direction of this anisotropy is rotating and, in reduced units, its magnitude  $\alpha$  is considerable ( $\sim 0.2$ ).

The vectorized approach requires us to include a total of 16 elements, arranged in two levels of  $2 \times 2$  matrices. The inner matrices each consist of elements for a given  $\gamma$  and  $\gamma'$

for all combinations of  $n$  and  $n'$ . The outer matrices obviously vary for  $\gamma$  and  $\gamma'$  then. Thus

$$\underline{D} = \begin{pmatrix} (k+n)^2(1+\alpha c_0) & \alpha(k+n)(k+n')c_{n'-n} & 0 & \alpha(k+n)(k+n')s_{n'-n} \\ \alpha(k+n)(k+n')c_{n-n'} & (k+n')^2(1+\alpha c_0) & \alpha(k+n)(k+n')s_{n-n'} & 0 \\ 0 & \alpha(k+n)(k+n')s_{n'-n} & (k+n)^2(1-\alpha c_0) & -\alpha(k+n)(k+n')c_{n'-n} \\ \alpha(k+n)(k+n')s_{n-n'} & 0 & -\alpha(k+n)(k+n')c_{n-n'} & (k+n')^2(1-\alpha c_0) \end{pmatrix}. \quad (54)$$

Given that  $\tilde{k} = -(n+n')/2$ , we obtain the eigenvalues

$$\tilde{\omega}^2 = \left(\frac{\delta n}{2}\right)^2 [1 \pm \alpha(c_{\delta n} \pm \sqrt{c_0^2 - s_{\delta n}^2})]. \quad (55)$$

This now gives us four eigenvalues at the Brillouin-zone boundary, split from a quadruple degeneracy of two dispersion relations with two polarizations each meeting at one point in  $\tilde{k}$ . Clearly in the undistorted case, we will obtain  $\tilde{\omega}^2 = \frac{1}{4}[1 \pm \alpha(\frac{1}{2} \pm \frac{1}{2})]$ . We interpret this answer as corresponding to two eigenmodes rotating with the helix that are split such that  $\tilde{\omega}^2 = \frac{1}{4}[1 \pm \alpha]$ , and two eigenmodes rotating against the helix that are unsplit so that both  $\tilde{\omega}^2 = \frac{1}{4}$ . We obtain the same result through numerical diagonalization of the  $A$  matrix for  $N \geq 2$ . For a distorted helix, given that  $c_0 = f\bar{e}$  and that  $s_1 = i(1/2 - ge^2)$  and  $c_1 = 1/2 - he^2$ , with constants  $f$ ,  $g$ , and  $h$ , we expect that

$$\tilde{\omega}^2 = \frac{1}{4} [1 \pm \alpha \{1/2 - he^2 \pm \sqrt{(fe)^2 + (1/2 - ge^2)^2}\}], \quad (56)$$

which corresponds to a large gap for the polarization that rotates along with the helix, given by  $\tilde{\omega}^2 = (1/4)[1 \pm \alpha(1 + (f^2 - g - h)\delta^2)]$ , and a small gap for the opposite helicity, given by  $\tilde{\omega}^2 \approx (1/4)[1 \pm \alpha(g - h - f^2)\delta^2]$ , corresponding to a gap of width  $\delta\omega = (1/2)\alpha(g - h - f^2)\delta^2$ . Since  $g - h - f^2$  is nonvanishing, in general, we expect that both gaps in the

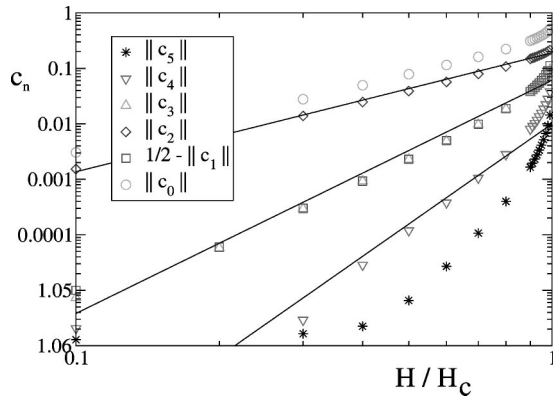


FIG. 8. Dependence of the Fourier coefficients  $c_n$  in a liquid cholesteric on an external uniform electric or magnetic field. Note that all  $c_n$  except for  $c_0$  go abruptly to zero for fields  $H$  greater than the critical field  $H_c$  (unlike in Fig. 7).

dispersion relation will be nonzero. These results correspond qualitatively to the scaling behavior observed in Figs. 9 and 10. Since the smaller gap is centered about the same value of  $\tilde{\omega}^2$  as the larger gap, we predict a *full* photonic band gap for a distorted helix at normal incidence, i.e., we expect that normally incident light of *any* polarization with frequencies within the band gap will be totally reflected.

We now extend the theory for splitting at the first Brillouin-zone boundary to higher orders. An important factor affects these anticrossings, namely, the gradual separation of the dispersion relations for eigenmodes that tend to point along  $\epsilon_{\perp}$  and eigenmodes that tend to point along  $\epsilon_{\parallel}$ . Since these two sets of eigenmodes experience a different effective refractive index, they have different slopes, which gives rise to two meeting points that gradually separate as we go to higher bands (corresponding to higher Brillouin zones in an extended-zone scheme). Furthermore, some of the higher crossings can take place away from the zone boundaries; however, those effects require mixing between two nearly orthogonal modes and are usually small. In practical terms, this means that rather than four-wave splitting, we must instead consider two-wave splitting at higher Brillouin-zone boundaries—a simpler problem, where the matrix  $\underline{D}$  becomes

$$\underline{D} = \begin{pmatrix} \left(\frac{\delta n}{2}\right)^2 (1 \pm \alpha c_0) & \mp \alpha \left(\frac{\delta n}{2}\right)^2 s_{\delta n} \\ \mp \alpha \left(\frac{\delta n}{2}\right)^2 s_{\delta n}^* & \left(\frac{\delta n}{2}\right)^2 (1 \pm \alpha c_0) \end{pmatrix}. \quad (57)$$

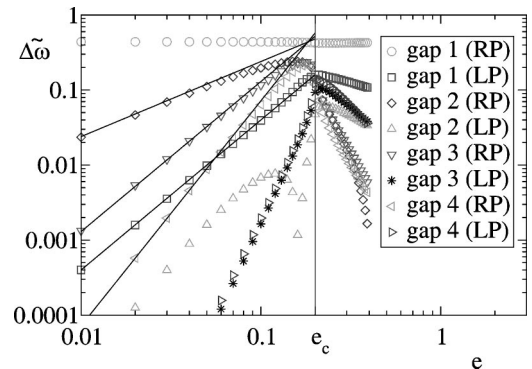


FIG. 9. Scaling of elastomer gaps with strain  $e$ . The lines are the results of our perturbation analysis.

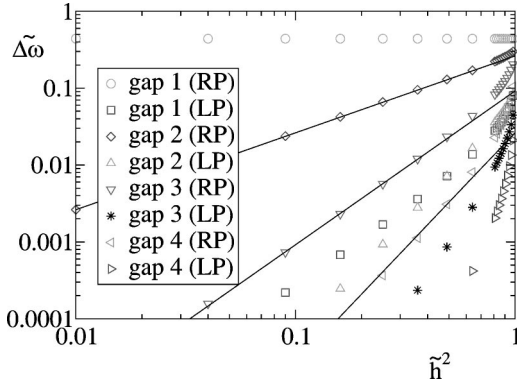


FIG. 10. Scaling of gaps in cholesteric liquids with reduced external field  $(H/H_c)^2$ . Note how the scaling corresponds to that seen in Fig. 9.

There are two pairs of eigenvalues:  $\tilde{\omega}^2 = (\delta n/2)^2 [1 - \alpha(c_0 \pm i s_{\delta n})]$  and  $\tilde{\omega}^2 = (\delta n/2)^2 [1 + \alpha(c_0 \pm i s_{\delta n})]$ , corresponding to a band gap of magnitude  $\delta\omega \approx (\delta n/2)\alpha |s_{\delta n}|$ .

### C. Experimental scaling of band gaps with mechanical strain

Of experimental interest is the *in vacuo* wavelength  $\Lambda$  of the light corresponding to a given  $\tilde{\omega}$  on the CE dispersion relation, particularly at the gaps. The previous definitions give  $\Lambda = p_0 / (\tilde{\omega} \sqrt{b} \lambda^{2/7})$ . Pitches  $p_0$  typically give a band in the visible region, so the initial wavelengths are  $\Lambda_0 = p_0 / \sqrt{b} \sim 500$  nm at  $\tilde{\omega} = 1/2$  and  $\lambda = 1$ , which allow us to write  $\Lambda = \Lambda_0 / (2\tilde{\omega} \lambda^{2/7})$ . Likewise the first-order de Vries gap is given by  $\Delta\Lambda \approx \Lambda_0 / \lambda^{2/7} \alpha$ . The higher-order gaps of the same polarization will have widths of  $\Delta\Lambda_n \approx C\Lambda_0 e^{n-1} / (n\lambda^{2/7})$ , where  $C$  is a prefactor of order unity that will depend on  $r$  and  $\alpha$ . For example, the second-order gap in rubber with  $r = 1.9$ ,  $\alpha = 0.18$ , and  $e = 0.1$  will be  $\Delta\Lambda_2 \approx 0.045\Lambda_0$ . For  $\Lambda_0 \approx 800$  nm, this implies that a second stop band for the light with a circular polarization in the same sense as the helix will be observed for  $\Lambda = 362$  nm to  $\Lambda = 398$  nm. We have taken for illustration in this paper  $\epsilon_{\parallel} = 3.3$  and  $\epsilon_{\perp} = 2.3$ , giving the extraordinary and ordinary refractive indices  $n_e = 1.82$  and  $n_o = 1.52$ . Then  $\alpha = 0.18$  and  $b = \frac{1}{2}(1/\epsilon_{\parallel} + 1/\epsilon_{\perp}) = 0.368$ . Actually,  $b$  does not appear in the calculation of band structures, but would be needed in constructing the light line  $\tilde{\omega} = \tilde{k} / \sqrt{b}$ , which limits propagation in a projected density of states diagram in the manner of Fink *et al.* [36].

## VI. OBLIQUE INCIDENCE

In Figs. 12 and 13, we show the full band structure, calculated by diagonalization of the matrix in Eq. (46), for arbitrary angles of propagation (i.e., arbitrary  $\mathbf{k}$  inside the cholesteric medium). As in electronic band structures, these photonic band structures traverse a range of  $\mathbf{k}$ 's to see how  $\omega$  varies in 3D. We increase or decrease a component of  $\mathbf{k}$  (either  $k_{\rho}$  and  $k_z$ ) until we hit a zone boundary, then “reflect back” or continue in a different direction. The lack of periodicity along  $\rho$  (perpendicular to the pitch axis) means that

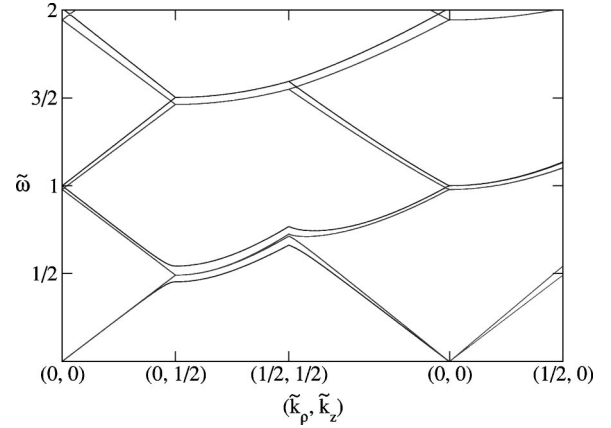


FIG. 11. Full dispersion relation at several directions of propagation in an ideal helix: (1) normal, (2) increasingly away from normal up to  $45^\circ$ , (3)  $45^\circ$  propagation for a decreasing magnitude of  $k$ , and (4)  $90^\circ$

each  $k_{\rho}$  is unique, and hence there is no zone boundary in that direction. However, the lowest bands (corresponding to visible light when the pitch is about one optical wavelength) will have a natural limit on  $k_{\rho}$  since *in vacuo*,  $\omega \geq c|k_{\rho}|$ , and in the cholesteric medium,  $\tilde{\omega} \geq (1 - \alpha)|\tilde{k}_{\rho}|$ . Qualitatively, these results mean that low frequencies must have a correspondingly low  $k_{\rho}$ .

Starting from  $(0,0)$  on the  $k$  axis, in the first segment only  $k_z$  increases, corresponding to the band structure for normal incidence. We can verify that the first parts of the full band structures we present, Figs. 11–13, are identical to Figs. 4–6, respectively. At the first zone boundary  $(1/2,0)$ , one observes the familiar stop bands. Then increasing  $k_{\rho}$  from 0 corresponds to a gradual tilt away from normal propagation along the helix axis, until the two components are equal at  $(1/2,1/2)$ . At that point, the  $\mathbf{k}$  corresponds to  $45^\circ$  propagation within the medium. We then gradually decrease the magnitude of  $\mathbf{k}$ , without changing the direction away from  $45^\circ$ . In the fourth and final segment of the axis, we look at the case of  $k_z = 0$ , corresponding to  $90^\circ$  propagation, along a direction perpendicular to the pitch axis (taken to be along  $\hat{y}$  for simplicity).

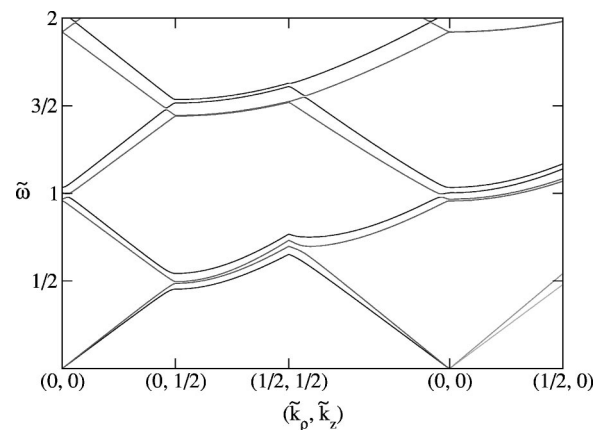


FIG. 12. Full dispersion relation at angles as in Fig. 11 for a helix distorted by a strain  $e = 1.1 < e_c$  ( $r = 1.9$ ).

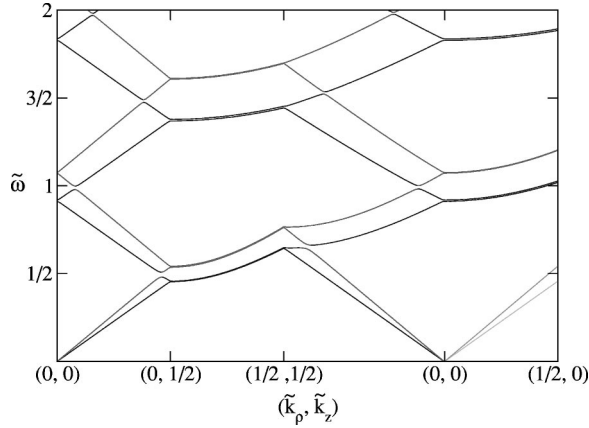


FIG. 13. Full dispersion relation at angles as in Fig. 11 for a helix distorted by a strain  $e = 1.3 > e_c$  ( $r = 1.9$ ).

*Ideal helix structures.* Figure 11 shows the band structure for an ideal cholesteric. Leaving normal incidence, one observes hints of a Bragg reflection even for the sense of polarization opposite to that of the helix. Oblique Bragg reflections are not unexpected from this periodic 1D structure acting as a grating coupler, but the stop band is weak for the other sense of polarization until one approaches  $45^\circ$ . Since the gap for the opposite sense circular polarized light sits inside that for the same sense polarized light, there is a stop band for *both* polarizations, which one might call, in the context of circularly polarized reflections, a “total” stop band. This contrasts strongly with the normally incident case, in which only one polarization experiences a reflection. More reflections would be visible if we were to sweep over a broader range of  $k_\rho$  values.

On moving away from normal incidence with constant  $k$ , the large, fundamental (de Vries) gap for the polarization that rotates with the helix scales as  $\alpha[1/2 - O(\theta^2)]$ . The smaller gap opening up for the opposite polarization scales as  $\theta^2$ . Bragg reflections correspond to the incoming and outgoing wave vectors being the same, modulo a reciprocal lattice vector, i.e.,  $\mathbf{k}^2 = (\mathbf{k} + \mathbf{G})^2$ , equivalently  $2\mathbf{k} \cdot \mathbf{G} = \mathbf{G}^2$ , yields  $\tilde{k}_z = \pm n/2$ ,  $n$  being an integer. At a given angle of propagation  $\theta > 0$  such that  $\tilde{k}_\rho = \tilde{k} \sin \theta$  and  $\tilde{k}_z = \tilde{k} \cos \theta$ , the reflections will take place at  $\tilde{k} = \pm n/(2 \cos \theta)$ , consistently with the above observations for the smaller gap.

Thus the dispersion relations for ideal cholesterics give the fundamental (de Vries) stop band trending upwards as the angle of incidence increases. This may provide an explanation for the success of lasing close to the upper band edge of cholesterics [17]. To wit, a lasing mode just above the upper frequency allowed at normal incidence (that is, at the lowest part of the upper band) will be forbidden above a critical angle. As one gets closer to the bottom of the upper part of the dispersion curve, the smaller the critical angle becomes. For a small enough critical angle, light will essentially be forced to propagate straight through the cholesteric medium, which will clearly assist in the collimation of light and the focusing of the energy of an emitter—more of the pumping power is utilized. This is an observation and interpretation by Kopp *et al.* [37].

The eigenmodes of a beam propagating at an angle  $90^\circ$  from normal will differ enormously from what was discussed previously for normal incidence. Of the two lowest eigenmodes, one has a dispersion relation given by  $\tilde{\omega}^2 = (1 + \alpha)\tilde{k}_\rho^2$  and a linear polarization along  $\hat{x}$  (assuming  $\mathbf{k} = 2q\tilde{k}_\rho\hat{y}$ ). This polarization corresponds to an  $\mathbf{E}$ , which points wholly along  $\hat{z}$ , the direction of the unvarying dielectric constant. The other polarization points all over space in a highly nontrivial manner, as a periodic function of  $y$  and  $z$ . This periodic variation costs a larger amount of energy than pointing along a constant direction. Nonetheless, since this polarization is able to take advantage of being able to direct its  $\mathbf{E}$  along a higher dielectric constant direction than the trivial polarization, it is lower in energy despite its twisting and turning. This can be confirmed by a visualization of the eigenfunctions, which we present elsewhere.

*Distorted helix structures.* The band structures for cholesteric elastomers distorted by strains of  $e = 1.1$  and  $e = 1.3$ , below and above the critical strain, respectively, are shown in Figs. 12 and 13.

Small stretching of a cholesteric rubber yields a smaller gap for the opposite handedness already at normal-incidence scaling as  $e$ , with the larger gap scaling as  $\alpha[1/2 - O(e^2)]$ . One can think of the opposite handedness gap arising because, in the rotating (de Vries) frame, with distortion of the helix there is effectively rotation backwards and thus a Fourier mode for the hitherto trivial polarization to couple to. Thus one sees in Fig. 12 a wider gap for the opposite handedness in the segment  $(0, 1/2) \rightarrow (1/2, 1/2)$  than in the nondistorted case. Above the critical point, Fig. 14, in the same interval, the two branches have gaps of almost equal size. Since there is no net rotation, but forward and backward rotation in equal measure, both handednesses couple to the photonic structure similarly, producing similar gaps. Note also that the primary stop band has moved away from the zone center, a result of the different slopes of the linear dispersion relations for the two branches in the segment increasing up from  $(0, 0)$ .

Inspection of the primary gaps in Figs. 11–13 shows that the frequencies at which the reflections take place is seen to increase as the angle away from normal incidence is increased, as is predicted by the previous considerations for elastic scattering, and observed experimentally by Takezoe *et al.* [38].

*Projected band structure.* The data in Figs. 11–13 is not directly applicable to experiment. The character of the eigenfunctions in the medium is not that of the corresponding waves outside (we have given the example of the eigenfunctions inside and outside the body at frequencies corresponding to the lower and upper edges of the fundamental stop band). The conversion, in general, of our eigenfunctions into exterior waves will be presented elsewhere.

The second reason is that not all angles of propagation inside the medium are accessible outside. It is a more complex form of the total internal reflection problem—when  $k_z \rightarrow 0$  outside the medium, the propagation there being grazing,  $k_z$  inside is not yet vanishing and the interior beam is far from being at grazing. The free space dispersion relation for light outside the medium,  $\omega = ck$ , can be reexpressed in our

reduced, dimensionless variables  $\tilde{\omega}$  and  $\tilde{k}$  to  $\tilde{\omega}=(1/\sqrt{b})\tilde{k}$ . Recall that  $b=\frac{1}{2}(1/\epsilon_1+1/\epsilon_2)$ . The in-plane component of the wave vector  $\tilde{k}_\rho$  is by boundary conditions continuous between the inside and outside of the body. Thus whatever the dispersion relation inside the body, at a given  $\tilde{k}_\rho$  the minimum possible  $\tilde{\omega}$  is  $\tilde{\omega}=1/\sqrt{b\tilde{k}}$ —the so-called light line.

Our stop bands do not extend to all angles, and thus do not produce a genuine gap in the density of states in frequency when taken over all angles. However, the restriction to a cone of angles in the material corresponding to angles  $0-\pi/2$  outside means that, measured from the outside, one can approach omnireflectivity in materials with only partial gaps. Fink *et al.* [36] take this view. We present detailed projections elsewhere.

## VII. CONCLUSIONS

An entirely different type of photonic material has been described and characterized. Not only is it self-assembling and easily available as large, defect-free single crystals, but it is highly deformable. Earlier descriptions [7,8,26,27] of its modified periodic dielectric structure have been used as the basis for calculating its band structure. Additional gaps arise and their widths scale in a well-understood fashion with the stretch applied to the material or the strength of the external field. The midgap frequencies shift position by large amounts comparable to their initial values. Total gaps (for both handednesses of circularly polarized light) arise. The band structure has been calculated for arbitrary obliquity. The extension of gaps to oblique incidence confirms the explanation and observation of Kopp *et al.* of low-threshold upper band lasing.

## ACKNOWLEDGMENTS

We thank A. Genack and P. Palfy-Muhoray for introducing us to lasing in cholesterics, and acknowledge valuable discussions with E.M. Terentjev, Y. Mao, H. Finkelmann, S.T. Kim, W. Stille, S. Shiyonovskii, P.D. Haynes, P.B. Littlewood, E.L. Thomas, H. Takezoe, and S. Johnson. P.A.B. acknowledges the support of the Winston Churchill Foundation. M.W. thanks the A. v. Humboldt Foundation for financial support.

## APPENDIX: MECHANICAL RELAXATION OF CHOLESTERIC ELASTOMERS

To calculate the free energy, substitute Eqs. (4) and (5) (and a similar expression for the current inverse step length tensor) in the free-energy expression, Eq. (3), to obtain an expression for the free energy  $F(\lambda, \lambda_{yy}, r, \phi, \phi_0)$  given in [26,27],

$$F = \frac{1}{2} \nu k_B T \left\{ \lambda^2 + \lambda_{yy}^2 + \frac{1}{\lambda^2 \lambda_{yy}^2} + \frac{r-1}{r} [\lambda^2 (r \cos^2 \phi_0 \sin^2 \phi - \sin^2 \phi_0 \cos^2 \phi) + \lambda_{yy}^2 (r \sin^2 \phi_0 \cos^2 \phi - \cos^2 \phi_0 \sin^2 \phi) - 2(r-1) \lambda \lambda_{yy} \cos \phi \cos \phi_0 \sin \phi \sin \phi_0] \right\}. \quad (\text{A1})$$

The local director orientation is determined by  $\partial \langle F \rangle / \partial \phi = 0$ . This rearranges to Eq. (6) for  $\phi(\phi_0)$ .

One can determine whether the  $\phi$  values given by Eq. (6) are stable by calculating  $\partial^2 \langle F \rangle / \partial \phi^2$  from Eq. (A1) and back-substituting Eq. (6) into the expression for the second derivative. We obtain

$$\frac{\partial^2 \langle F \rangle}{\partial \phi^2} = \frac{1}{4r\lambda\lambda_{yy}} \nu k_B T \{ [(r+1)(\lambda^2 - \lambda_{yy}^2) + (r-1)(\lambda^2 + \lambda_{yy}^2) \cos 2\phi_0]^2 + 4(r-1)^2 \lambda^2 \lambda_{yy}^2 \sin^2 2\phi_0 \} \left( \frac{\sin 2\phi}{\sin 2\phi_0} \right). \quad (\text{A2})$$

Since the quantities in braces are positive definite, the sign of  $\partial^2 \langle F \rangle / \partial \phi^2$  will be given by the sign of  $\sin 2\phi / \sin 2\phi_0$ . Thus, when  $\sin 2\phi$  and  $\sin 2\phi_0$  are of the same sign, the second derivative will be positive, corresponding to a local minimum in free energy. One can then use Eq. (6) and this stability analysis to obtain  $\cos 2\phi$  and  $\sin 2\phi$ , which are thus given by

$$\sin 2\phi = \frac{(r-1)\lambda\lambda_{yy} \sin 2\phi_0}{\sqrt{a_1^2 - 4r\lambda^2\lambda_{yy}^2}} \quad (\text{A3})$$

and

$$\cos 2\phi = -\frac{\lambda_{yy}^2 - r\lambda^2 + (r-1)(\lambda^2 + \lambda_{yy}^2) \sin^2 \phi_0}{\sqrt{a_1^2 - 4r\lambda^2\lambda_{yy}^2}}, \quad (\text{A4})$$

where  $a_1 = r\lambda^2 + \lambda_{yy}^2 - (r-1)(\lambda^2 - \lambda_{yy}^2) \sin^2 \phi_0$ . These are required to generate the harmonics for the band-structure analysis. We can substitute these values back into Eq. (A1) to obtain  $F(\lambda, \lambda_{yy}, r, \phi_0)$ . We then coarse grain this free energy over one turn of the helix to give  $F(\lambda, \lambda_{yy}, r) = \int_0^\pi d\phi_0 F(\lambda, \lambda_{yy}, r, \phi_0)$ . Given a fixed value for  $\lambda$  and  $r$ , we can find the minimum-energy value of  $\lambda_{yy}$  by setting  $\partial F / \partial \lambda_{yy} = 0$ . The relaxation  $\lambda_{yy}(\lambda)$  is shown in Fig. 14.

If we assume that  $\lambda_{yy}$  is a power law in terms of  $\lambda$  in the limit of small strains  $e = \lambda - 1 \rightarrow 0$ , then we can use a perturbation analysis to obtain the exponent. First, energy minimization is explicitly

$$0 = \pi - \frac{\pi}{\lambda^2 \lambda_{yy}^4} + \frac{\pi}{4} \frac{(r-1)^2}{r} + \frac{r-1}{r} \int_0^{\pi/2} d\phi_0 \left[ (r \sin^2 \phi_0 + \cos^2 \phi_0) \cos 2\phi - \frac{r-1}{2} \frac{\lambda}{\lambda_{yy}} \sin 2\phi_0 \sin 2\phi \right], \quad (\text{A5})$$

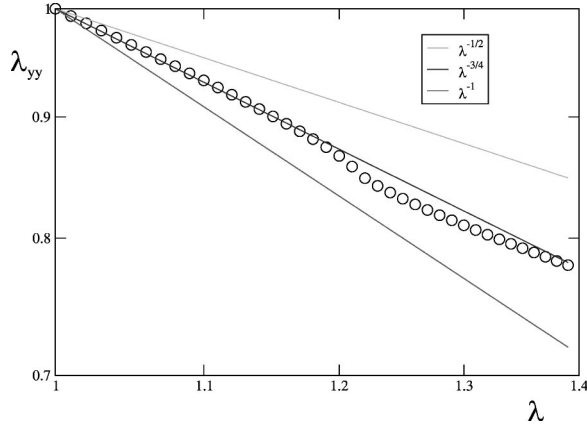


FIG. 14. Numerical calculation of the contraction of a cholesteric elastomer  $\lambda_{yy}$  as a function of the applied uniaxial strain  $\lambda$  for  $r=1.9$  ( $\lambda_c \approx 1.19$ ). An exponent of  $-3/4$  gives a good fit for  $\lambda_{yy}(\lambda)$  up to large strains, an exponent close to the exact, small strain value of  $-5/7$ .

Next, substitution of the appropriate expressions for  $\sin 2\phi$  and  $\cos 2\phi$ , Eqs. (A3) and (A4), yields an expression for  $\lambda_{yy}(\lambda)$ ,

$$\frac{\pi}{4} \frac{(r+1)^2}{r} - \frac{\pi}{\lambda^2 \lambda_{yy}^4} - \frac{r-1}{r} \int_0^{\pi/2} d\phi_0 \left\{ \frac{a_1 [1 + (r-1) \sin^2 \phi_0] - 2r\lambda^2}{\sqrt{a_1^2 - 4r\lambda^2 \lambda_{yy}^2}} \right\} = 0. \quad (\text{A6})$$

Equation (A6) may be written in a simplified form such that

$$\frac{\pi}{4} \frac{(r+1)^2}{r} - \frac{\pi}{\beta^2 \lambda^6} - \frac{r-1}{r} \int_0^{\pi/2} d\phi_0 \left\{ \frac{a'_1 [1 + (r-1) \sin^2 \phi_0] - 2r}{\sqrt{a_1'^2 - 4r\beta}} \right\} = 0, \quad (\text{A7})$$

where  $a'_1 = a_1/\lambda^2$  and  $\beta = \lambda_{yy}^2/\lambda^2$ . Expanding for  $e \ll 1$ , we have  $\lambda = 1 + e$  and  $\beta = \lambda^{-\varpi} \approx 1 - \varpi e$ , which can be substituted into Eq. (A7) to produce an expression to the first order in  $e$ , namely,

$$\pi \left[ \frac{(r+1)^2}{4r} - 1 + (6 - 2\varpi)e \right] - \frac{\pi}{4r} [(r-1)^2 - r\varpi e] = 0. \quad (\text{A8})$$

The left-hand side vanishes when  $\varpi = 24/7$  (to the first order), which, given the definitions of  $\beta$  and  $\varpi$ , implies that  $\lambda_{yy} = \lambda^{-5/7}$ . Of course, this scaling is only valid for small  $e$ . There is a critical strain, denoted by  $e_c$ , and an accompanying critical deformation  $\lambda_c = 1 + e_c$ , at which the twist walls created by the strain become thermodynamically unfavorable. At that point the director fails to accumulate any net cholesteric twist and oscillates back and forth around  $\phi = 0$ . Twist walls must be lost by a topological process such as the growth of disclination loops. Experimentally the dynamics of approaching the untwisted state suggest such a complex process. There will also be a crossover from the scaling behavior  $\lambda_{yy} \sim \lambda^{-5/7}$  for small strain, to the classical isotropic response  $\lambda_{yy} \sim \lambda^{-1/2}$  for large strain.

In Eq. (6) one sees that  $\tan 2\phi$  will only diverge if the denominator crosses zero, so the critical strain corresponds to the point at which the denominator is guaranteed to be greater than or equal to zero. Thus

$$\nabla_{\phi_0} (r-1)(\lambda^2 + \lambda_{yy}^2) \cos 2\phi_0 + (r+1)(\lambda^2 - \lambda_{yy}^2) \geq 0. \quad (\text{A9})$$

Since  $\cos 2\phi_0$  is bounded between  $\pm 1$ , Eq. (A9) requires

$$(r+1)(\lambda^2 - \lambda_{yy}^2) \geq (r-1)(\lambda^2 + \lambda_{yy}^2). \quad (\text{A10})$$

If it is assumed that  $e \ll 1$ , and that  $\lambda_{yy} \sim \lambda^{-\kappa}$ , this implies

$$(r+1)(1 + \kappa)e \geq (r-1)[1 + (1 - \kappa)e]. \quad (\text{A11})$$

Thus, the critical strain is

$$e_c \approx \frac{r-1}{(r+1)(\kappa+1) + (r-1)(\kappa-1)}. \quad (\text{A12})$$

Expanding the expression for  $e_c$  to the first order in  $r-1$  yields the result  $e_c = (r-1)/[2(1 + \kappa)]$ . Inspection of Fig. 14 suggests that  $\kappa \approx 3/4$ , a value close to the initial  $\kappa = 5/7$ , which is strictly correct only for  $\lambda \rightarrow 1$ . As a result, it can easily be shown that  $\lambda_c \approx r^{2/7}$ , to the first order.

Although obtaining an exact analytic solution is infeasible, we can find the critical values for  $F$  (with respect to  $\lambda_{yy}$ ) numerically, as shown in Fig. 14. We confirm that, for parameter values of interest (e.g.,  $r=1.9$ ,  $1 \leq \lambda \leq 1.4$ ), a minimum-energy state occurs at values of  $\lambda_{yy} \approx \lambda^{-3/4}$  for  $e < e_c$ . There is also evidently a crossover to the classical scaling  $\lambda_{yy} \approx \lambda^{-1/2}$  for  $e > e_c$ .

- [1] E. Yablonovitch and T.J. Gmitter, Phys. Rev. Lett. **63**, 1950 (1989).  
 [2] E. Ozbay, A. Abeyta, G. Tuttle, N. Tringides, R. Biswas, C.T. Chan, C.M. Soukoulis, and K.M. Ho, Phys. Rev. B **50**, 1945 (1994).

- [3] J.E. Wijnhoven and W.L. Vos, Science **281**, 802 (1998).  
 [4] A. Urbas, Y. Fink, and E.L. Thomas, Macromolecules **32**, 4748 (1999).  
 [5] M. Muller, R. Zentel, T. Maka, S.G. Romanov, and C.M.S. Torres, Adv. Mater. **12**, 1499 (2000).

- [6] H. de Vries, *Acta Crystallogr.* **4**, 219 (1951).
- [7] R.B. Meyer, *Appl. Phys. Lett.* **12**, 281 (1968).
- [8] P.-G. de Gennes, *Solid State Commun.* **6**, 163 (1968).
- [9] S.G. Chou, L. Cheung, and R.B. Meyer, *Solid State Commun.* **11**, 277 (1972).
- [10] D.W. Berreman and T.J. Scheffer, *Phys. Rev. Lett.* **25**, 577 (1970).
- [11] S. John, *Phys. Rev. Lett.* **58**, 2486 (1987).
- [12] W. Stille, Ph.D. Thesis, University of Clausthal, 1978.
- [13] E. Yablonovitch, *Phys. Rev. Lett.* **58**, 2059 (1987).
- [14] M.D. Tocci, M. Scalora, M.J. Bloemer, J.P. Dowling, and C.M. Bowden, *Phys. Rev. A* **53**, 2799 (1996).
- [15] O. Painter, R.K. Lee, A. Scherer, A. Yariv, J.D. O'Brien, P.D. Dapkus, and I. Kim, *Science* **284**, 1819 (1999).
- [16] J.P. Dowling, M. Scalora, M.J. Bloemer, and C.M. Bowden, *J. Appl. Phys.* **75**, 1896 (1994).
- [17] V.I. Kopp, B. Fan, H.K.M. Vithana, and A.Z. Genack, *Opt. Lett.* **23**, 1709 (1998).
- [18] B. Taheri and P. Palfy-Muhoray, in *ALCOM Symposium*, Cuyahoga Falls, 1999 (unpublished).
- [19] H. Finkelmann, S.T. Kim, A. Munoz, P. Palfy-Muhoray, and B. Taheri, *Adv. Mater.* **13**, 1069 (2001).
- [20] S.T. Kim and H. Finkelmann, *Macromol. Rapid Commun.* **22**, 429 (2001).
- [21] P.A. Bermel and M. Warner, *Phys. Rev. E* **64**, 010702 (2001).
- [22] K. Busch and S. John, *Phys. Rev. Lett.* **83**, 967 (1999).
- [23] R. Dreher, *Solid State Commun.* **13**, 1571 (1973).
- [24] R. Dreher, *Solid State Commun.* **12**, 519 (1973).
- [25] S. Shtrikman and M. Tur, *J. Opt. Soc. Am.* **64**, 1178 (1974).
- [26] M. Warner, E.M. Terentjev, R.B. Meyer, and Y. Mao, *Phys. Rev. Lett.* **85**, 2320 (2000).
- [27] Y. Mao, E.M. Terentjev, and M. Warner, *Phys. Rev. E* **64**, 041803 (2001).
- [28] P.-G. de Gennes and J. Prost, *The Physics of Liquid Crystals* (Clarendon Press, Oxford, 1993).
- [29] R. Dreher and G. Meier, *Phys. Rev. A* **8**, 1616 (1973).
- [30] V.I. Kopp and A.Z. Genack, in *Photonics West SPIE Conference on Organic Photonic Materials and Devices*, edited by B. Kippelen (SPIE, Bellingham, WA, 1999).
- [31] K.M. Ho, C.T. Chan, and C.M. Soukoulis, *Phys. Rev. Lett.* **65**, 3152 (1990).
- [32] R.D. Meade, A.M. Rappe, K.D. Brommer, J.D. Joannopoulos, and O.L. Altherhand, *Phys. Rev. B* **48**, 8434 (1993).
- [33] R. Hornreich *et al.*, *Phys. Rev. E* **47**, 2067 (1993).
- [34] E. Anderson *et al.*, *LAPACK: A Portable Linear Algebra Library for High Performance Computers* (SIAM, Philadelphia, 1995).
- [35] P. Cicutta, A.R. Tajbakhsh, and E.M. Terentjev, *Phys. Rev. E* **65**, 051704 (2002).
- [36] Y. Fink, J.N. Winn, S. Fan, C. Chen, J. Michel, J.D. Joannopoulos, and E.L. Thomas, *Science* **282**, 1679 (1998).
- [37] V.I. Kopp, A.Z. Genack, and Z.-Q. Zhang, *Phys. Rev. Lett.* **86**, 1753 (2001).
- [38] H. Takezoe, Y. Ouchi, M. Hara, A. Fukuda, and E. Kuze, *Jpn. J. Appl. Phys., Part 1* **22**, 1080 (1983).